Unclassified

SECURITY CLASSIFICATION OF THIS PAGE

(2)

ICUMENTATION PAGE

Form Approved
OMB No. 0704-0188

AD-A213 679

1b. RESTRICTIVE MARKINGS

2 ...ION / DOWNGRADING SCHEDULE

3. DISTRIBUTION / AVAILABILITY OF REPORT
Approved for public release; distribution is unlimited

4. PERFORMING ORGANIZATION REPORT NUMBER(S)

5. MONITORING ORGANIZATION REPORT NUMBER(S)
AFOSR-TR- 89-1275

6a. NAME OF PERFORMING ORGANIZATION
Dept. of Aeronautics & Astronautics, MIT,

6b. OFFICE SYMBOL (If applicable)

7a. NAME OF MONITORING ORGANIZATION
AFOSR/NA

6c. ADDRESS (City, State, and ZIP Code)
Cambridge, MA 02139

7b. ADDRESS (City, State, and ZIP Code)
Building 410, Bolling AFB DC 20332-6448

8a. NAME OF FUNDING / SPONSORING ORGANIZATION
AFOSR/NA

8b. OFFICE SYMBOL (If applicable)
NA

9. PROCUREMENT INSTRUMENT IDENTIFICATION NUMBER
AFOSR-86-0119

8c. ADDRESS (City, State, and ZIP Code)
Building 410, Bolling AFB DC 20332-6448

10. SOURCE OF FUNDING NUMBERS

PROGRAM ELEMENT NO.	PROJECT NO.	TASK NO	WORK UNIT ACCESSION NO.
61102F	2308	A1	

11. TITLE (Include Security Classification)
Annual report on physical process in MPD plasmas (U)

12. PERSONAL AUTHOR(S)
Daniel Hastings

13a. TYPE OF REPORT	13b. TIME COVERED	14. DATE OF REPORT (Year, Month, Day)	15. PAGE COUNT
~~Annual~~ FINAL	FROM 5-1-88 TO 4-31-89	7/19/89	40

16. SUPPLEMENTARY NOTATION

17. COSATI CODES		
FIELD	GROUP	SUB-GROUP

18. SUBJECT TERMS (Continue on reverse if necessary and identify by block number)
MPD plasmas, advanced thrusters, plasma physics

19. ABSTRACT (Continue on reverse if necessary and identify by block number)

Magnetoplasmadynamic, or MPD, thrusters are a promising method of propulsion for a variety of different space missions. This research develops and analyzes a numerical simulation of a quasi one dimensional model for an MPD thruster. A finite difference scheme is used to integrate the fluid equations for each species and a magnetic field equation derived from Maxwell's laws. The model includes separate electron and heavy species temperatures, varying conductivity, varying ionization fraction, collisional energy transfer between heavy particles and electrons, averaged viscosity and ambipolar diffusion, and electron heat conduction, Both constant area and variable area channels are examined. The applied current in the cases studied ranges from 79.6 $\frac{\text{kAmp}}{\text{meter depth}}$ to 159 $\frac{\text{kAmp}}{\text{meter depth}}$ for an inlet mass flow of 0.5 $\frac{\text{kg}}{\text{m}^2\text{.sec}}$. It is shown that thermal equilibrium is not a valid assumption in a typical thruster. It is also found that viscosity plays a significant role in determining thruster performance. Area variation is also found to have a significant effect on performance.

20. DISTRIBUTION / AVAILABILITY OF ABSTRACT
☒ UNCLASSIFIED/UNLIMITED ☐ SAME AS RPT. ☐ DTIC USERS

21. ABSTRACT SECURITY CLASSIFICATION
Unclassified

22a. NAME OF RESPONSIBLE INDIVIDUAL	22b. TELEPHONE (Include Area Code)	22c. OFFICE SYMBOL
Dr. Mitat Birkan	(202) 767-4938	AFOSR/NA

DD Form 1473, JUN 86 *Previous editions are obsolete.* SECURITY CLASSIFICATION OF THIS PAGE

Unclassified

89 10 24 086

Physical Processes in MPD plasmas

Manuel Martinez-Sanchez and Daniel Hastings
Dept of Aeronautics and Astronautics
37-441,MIT,Cambridge, MA 02139
(617)-253-0906

Submitted to
Dr. M. Birkans
AFOSR/NA, Bolling AFB
DC, 20332-6448

Period of Performance: May 1, 1988- April 31, 1989

Co-Principal Investigator: Daniel Hastings

July 19, 1989

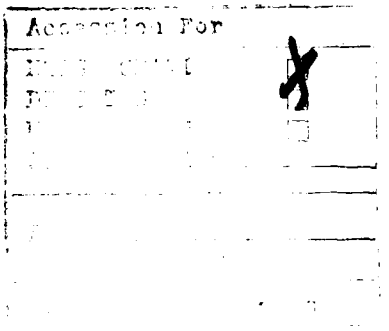

A-1

Summary

In the last year the work on this grant has involved the efforts of Eric Sheppard in pursuit of his doctoral degree. Additionally Jean-Marc Chanty was supported for a time on this grant. The work of Eric Sheppard is summarized in the following attachment. The work of Jean-Marc Chanty is a continuation of the research presented in the attached paper. In addition Eli Niewood received partial support from this grant. His work has resulted in a paper to be submitted for publication. A summary of his work and the paper is attached.

Nonequilibrium and Radiation in MPD Plasmas

AFOSR Grant 86-0019

Manuel Martinez-Sanchez

Dept of Aeronautics and Astronautics

MIT,Cambridge, MA 02139

This is a summary of work contributed by Eric J. Sheppard, graduate student, under the AFOSR grant. Some early results were reported in "Spectroscopic Investigation of the Exit Plane of an MPD Thruster" (Kilfoyle, Martinez, Heimerdinger and Sheppard; IEPC paper # 88-027).

The basic co-axial MPD thruster is shown in figure 1. The plasma is accelerated primarily by the Lorenz force, and is heated by Ohmic dissipation. For this analysis, a 1-D approach is taken, represented by the idealized set-up shown in figure 2. That is, in this work, the flow through a long, thin channel is investigated, with particular interest in the radiative emission from the plasma. Figures 3 and 4 show some of the detailed physics that have been included in models at MIT; most of these will be in the final model developed by this work. The areas of focus here are radiation, inelastic collisions, and ambipolar diffusion. Following is a discussion of work done, and under way.

A finite-rate approach to the kinetics concerning level populations in atoms was motivated by the earlier experimental work of Heimerdinger (J. J. Heimerdinger, *Fluid Mechanics in a Magnetoplasmadynamic Thruster*, Doctoral dissertation, Massachusetts Institute of Technology, Dept. of Aeronautics and Astronautics, 1988) and Kilfoyle (D. B. Kilfoyle, *Spectroscopic Analysis of a Magnetoplasmadynamic Arcjet*, Masters thesis, M.I.T., Dept. of Aero. & Astro., 1988), who took spectroscopic measurements at the exit plane of an MPD thruster. There is interest both in the detailed population rates and the spectral intensities of line radiation emitted from electronically excited atoms.

First, the effect of inelastic collisions (excitation/de-excitation, ionization/recombination), line radiation, and ambipolar diffusion (to the walls, where recombination to the ground occurs) on the populations of the excited energy levels in both argon (atom and ion) and hydrogen was investigated. This is referred to as the CRD model, and is also used for calculating ionization fractions. The initial CRD model is applicable to a steady-state, static discharge in a plasma, and is based on the formulation presented in several sources, in particular Mitchner and Kruger (*Partially Ionized*

Gases, Chapter 9). Continuity equations for number densities n, with e representing the ion (since $n_e = n_i$), $k = 1$ the ground state atom, and $k > 1$ the excited states are:

$$\begin{aligned}
\frac{\partial n_e}{\partial t} + \nabla \cdot (n_e \vec{u}) &= \dot{n}_e - \frac{D_a n_e}{L^2} \\
\frac{\partial n_{k=1}}{\partial t} + \nabla \cdot (n_{k=1} \vec{u}) &= \dot{n}_{k=1} + \frac{D_a n_e}{L^2} \\
\frac{\partial n_{k>1}}{\partial t} + \nabla \cdot (n_{k>1} \vec{u}) &= \dot{n}_{k>1}
\end{aligned}$$

For the steady-state, static case, the left hand side of each of these equations is identically equal to zero. D_a is the ambipolar diffusion coefficient, L is an equivalent diffusion radius, and the rate equations are:

$$\begin{aligned}
\dot{n}_e &= n_e \sum_k n_k S_{kc} - n_e^2 \sum_k (n_e S_{ck} + A_{ck}\beta_{ck}) \\
\dot{n}_k &= n_e \sum_{j<k} n_j S_{jk} - n_k [\sum_{j<k} (n_e S_{kj} + A_{kj}\beta_{kj}) + n_e (\sum_{l>k} (S_{kl}) + S_{kc})] \\
&\quad + \sum_{l>k} n_l (n_e S_{lk} + A_{lk}\beta_{lk}) + n_e^2 (n_e S_{ck} + A_{ck}\beta_{ck})
\end{aligned}$$

Here, the S terms are calculated collisional rate terms and the A terms are transition probabilities for the radiation events. The ratio of radiation lost from the volume to the total radiation emitted is denoted by the radiative escape factor, β, which ranges from 0 (optically thick) to 1 (optically thin). In all of the terms, the subscripts refer to processes which involve a change from the level denoted by the first index to the second (c here refers to the continuum, or ion state). It is important to note that this is not a self-consistent problem as stated - the temperatures are reasonably chosen, but still arbitrary, as is the total number density. Also, only k equations are solved for the $k + 1$ populations (the k levels of the atom and the ion/electron; the ground state ($k = 1$) equation is dropped) - the electron density is arrived at iteratively, as it appears as a cubic term in the equations.

Results show that radiation and diffusion effects on the populations of excited levels are largest (relative to a purely collisional model) at low temperatures and number densities, with diffusion (across a typical 2 cm MPD channel) having the larger influence. Ionization fractions may be lower than thermal equilibrium results by several orders of magnitude under these conditions. Figure 5 shows typical population results on a Boltzmann plot for argon. The solid line represents what

the populations curve would look like if all the levels were in Saha equilibrium. The slope here is an indicator of the electron temperature, and is in general agreement with the equilibrium curve. However, for smaller diffusion radii, the mid-range of energy levels may not reflect the proper temerature. This difference is even more dramatic in the argon atom. In both, only the uppermost levels are always in equilibrium with the electrons.

Next, a 2-gas static model was developed. This work is designed to follow up on a procedure used by Kilfoyle and Heimerdinger. The argon plasma was seeded with hydrogen in an attempt to use hydrogen lines for the spectrographic diagnostics. A 2-gas, 2-level each model is in use. The formulation of the problem is similar to the 1-gas static model, with the only interaction between the two gases coming from electronic collisions. The individual $\dot{n}_k$ formulations are the same as used earlier, with the complete set of equations:

$$\begin{aligned}
\sum_j n_j^{s1} + \sum_k n_k^{s2} + n_e &= n_{tot} \\
\frac{\partial n_e^{s1}}{\partial t} + \nabla \cdot (n_e^{s1}\vec{u}) &= \dot{n}_e^{s1} - \frac{D_a^{s1} n_e^{s1}}{L^2} \\
\frac{\partial n_e^{s2}}{\partial t} + \nabla \cdot (n_e^{s2}\vec{u}) &= \dot{n}_e^{s2} - \frac{D_a^{s2} n_e^{s2}}{L^2} \\
\frac{\partial n_{j>1}^{s1}}{\partial t} + \nabla \cdot (n_{j>1}^{s1}\vec{u}) &= \dot{n}_{j>1}^{s1} \\
\frac{\partial n_{k>1}^{s2}}{\partial t} + \nabla \cdot (n_{k>1}^{s2}\vec{u}) &= \dot{n}_{k>1}^{s2} \\
(1-\chi)(\sum_j n_j^{s1} + \xi n_e) &= \chi(\sum_k n_k^{s2} + (1-\xi) n_e)
\end{aligned}$$

Here, $s1$ and $s2$ denote the two gases used. The factor χ is the fraction: $\frac{\rho^{s2}}{\rho}$, which is a user input, and ξ is $\frac{n_e^{s1}}{n_e}$, which is solved for along with the populations.

At some temperatures the ionization fraction calculated for hydrogen was smaller than that for argon, and at the number densities looked at (around $10^{15} cm^{-3}$) the difference between the two was not very large. This seemed counter-intuitive at first, but it turned out to be due to what is referred to here as the crossover temperature. That is, the difference in the degeneracies of H and A mean that there is a temperature (around 10100 K) where, for any n_{tot}, the (Saha thermal) equilibrium ionization fractions are equal: $\alpha_A = \alpha_H$. Below this crossover temperature, $\alpha_A < \alpha_H$, and above it, $\alpha_A > \alpha_H$. The crossover temperature, T_x, can be found from the Saha equation by setting $\alpha_{s_1} = \alpha_{s_2}$ for any two gases s_1 and s_2 (where $\theta = \frac{E_{ion}}{k}$, g is a degeneracy, i represents the ion, and 1 the ground state atom):

$$\frac{\theta_2 - \theta_1}{T_x} = \ln([\frac{g_i}{g_1}]^{s_1}[\frac{g_1}{g_i}]^{s_2})$$

Figure 6 shows the ionization fractions of A and H as functions of the electron temperature, calculated by the Saha equilibrium equation. The vertical line is drawn at about the theoretical crossover temperature for A and H, and the total number density increases by one order of magnitude with every pair of lines moving to the right.

Results from the 2-gas model for low mass fractions (hydrogen:total) show that the hydrogen acts as a fairly poor seed (it doesn't increase the ionization fraction much) at the temperatures below T_x, and in fact it lowers α a little at above T_x. This may be good, assuming that the only interaction between the two gases is between their electrons, because the addition of the hydrogen has a small effect on the bulk plasma properties (i.e., conductivity). However, we have the possible advantage of gaining access to hydrogen lines for the spectrometer.

Channel-flow physics need to be included to study the effects of a plasma out of thermal equilibrium moving through a discharge (i.e., what we see in an MPD thruster). This makes the work self-consistent; that is, the temperatures and total density are no longer arbitrarily input, but are calculated in the channel. A 1-D flow model (a space-marching scheme following Niewood's work (E. Niewood, *Transient One Dimensional Numerical Simulation of Magnetoplasmadynamic Thrusters*, Masters thesis, MIT, Dept. of Aero. & Astro., 1989)) is being developed. This is a two-temperature (one temperature for the light electrons (T_e), one temperature for the heavies: the ions and neutrals (T_g)), one speed model, which includes ionization and recombination and area variation. Radiative decay, and detailed continuity equations for the excited levels have been added. The steady-state 1-D equations in non-dimensional form are (ξ is the nondimensional axial coordinate) :

$$\rho u a = 1$$

$$\frac{d\alpha}{d\xi} = a(\dot{\alpha} - D)$$

$$\frac{d\beta_1}{d\xi} = a(\dot{\beta} + D)$$

$$\frac{d\beta_{k>1}}{d\xi} = a\dot{\beta}_{k>1}$$

$$\rho u \frac{du}{d\xi} + \frac{d}{d\xi}[p + b^2] = \tau$$

$$\rho \frac{d\alpha T_e}{d\xi} - (\gamma - 1)\alpha T_e \frac{d\rho}{d\xi} = (\gamma - 1)[-a\theta_i \dot{\alpha} + \frac{2J^2}{R_m u}]$$

$$\rho \frac{dT_g}{d\xi} - (\gamma - 1)T_g \frac{d\rho}{d\xi} = (\gamma - 1)\frac{\Phi - \dot{R}}{u}$$

Where τ is the viscous force; Φ is the viscous dissipation; α is the ionization fraction ($\frac{n_e}{n_{tot}}$); D is the ambipolar diffusion; $\beta_k = \frac{n_k}{n_{tot}}$, where n_k is the number density of the level (level 1 is the ground state); $\dot{R}$ is the radiative energy loss from excited species; and $R_m = \mu_o \sigma u L$ is the magnetic Reynolds number. The $\dot{\alpha}$-like terms represent the net kinetic rate of population of the level involved, and it is assumed that diffusion to the walls results in a recombination event resulting in a ground state atom. Using these equations, along with the definition of the speed of sound (c_s) and Mach number (M), an equation of state, and Ohm's law, the following expression for the velocity gradient is found:

$$\frac{du}{d\xi} = \frac{-aM^2[\frac{c_s}{Ma^2}\frac{da}{d\xi} + (\gamma - 1)(\frac{\Phi - \dot{R}}{u} - a\theta_i \dot{\alpha}) + \frac{2\gamma}{u}(ub - \frac{\gamma - 1}{\gamma}E)\frac{db}{d\xi} - \tau]}{M^2 - 1} \qquad (1)$$

This form poses a numerical difficulty when integrating from the inlet, in that both the numerator and denominator must go to zero simultaneously. This problem is avoided by using L'Hopital's rule to evaluate the derivative at the sonic point ($M = 1$), and integrating forward to the exit plane. If the proper condition is met there, namely, $b = 0$, then a back-integration is initiated from the sonic point to obtain the inlet conditions. At present, this is being carried out for a 2-level (one excited state and the ground) argon atom; some results are shown in Figure 7. This same approach was used earlier in a one-fluid (MHD) model, and figure 8 shows the variation of the sonic passage point with the magnetic Reynolds number. This behavior validates the inner-outer expansion used by Martinez in an earlier publication. (The Structure of Self-Field Accelerated Flows", AIAA-87-1065)

The expediency of this 1-D approach has a shortcoming; all the transverse gradients, which are critical for radiative transfer, must be approximated algebraically. To this end, a brief examination of boundary layers in the MPD will be made. Analytical work has started, and a simple numerical model is being tested.

The final step is to analyze the spectral intensities of hydrogen and argon lines; this to be compared to previous experimental work, and used in guiding future experimental diagnostic methods. In particular, the choices of seeding options and spectral lines to observe, and the relationship between the intensities measured and the temperatures and (derived) number densities of the plasma will be studied. Thus, the result of this study will be a 1-D numerical model (axial flow with transverse effects either assumed or approximated in algebraic form) for an argon plasma seeded with hydrogen in an MPD thruster. Multi-level models will be used in order to capture the details of the radiating excited levels of interest.

Preliminary work agrees with the results of Niewood, that there are two distinct temperatures, and that the ionization rate terms do have a significant effect on the flow variables. Future work will extend the existing model, as well as add in more of the processes shown in figures 3 and 4.

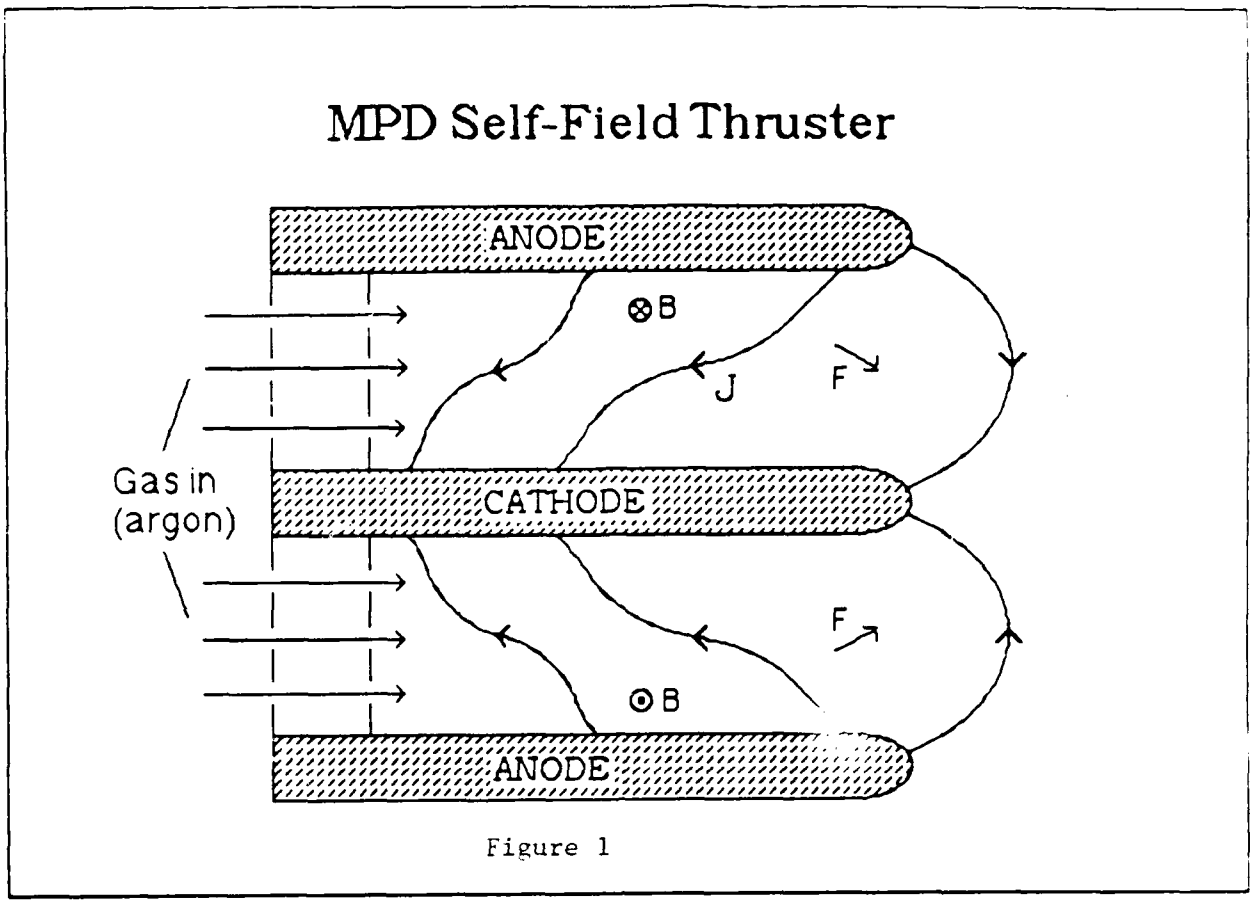

Figure 1

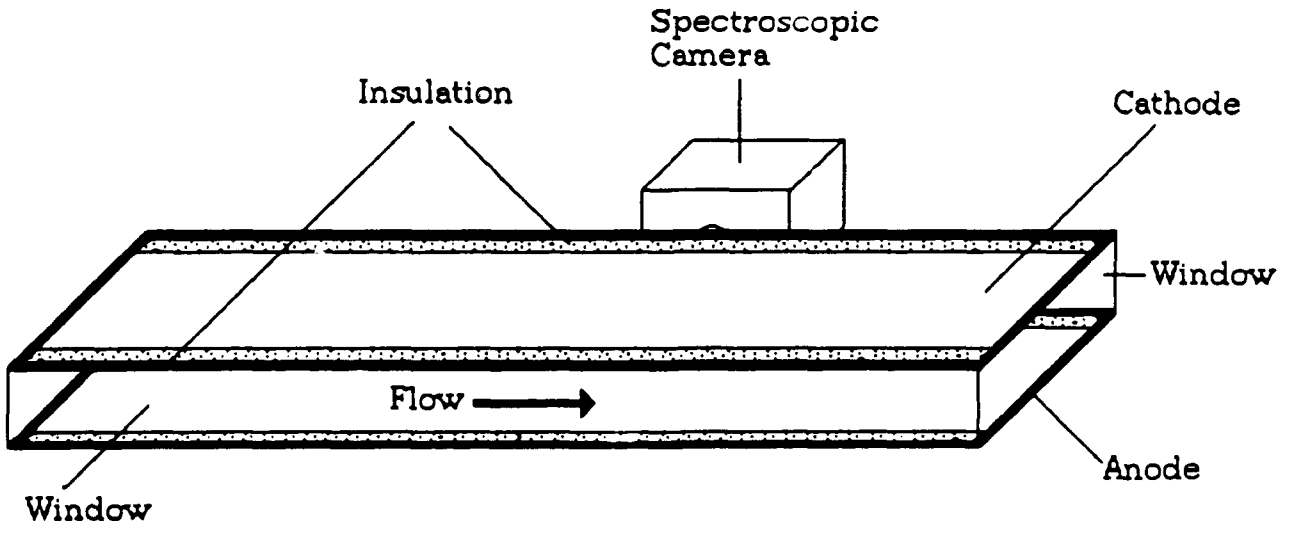

Figure 2

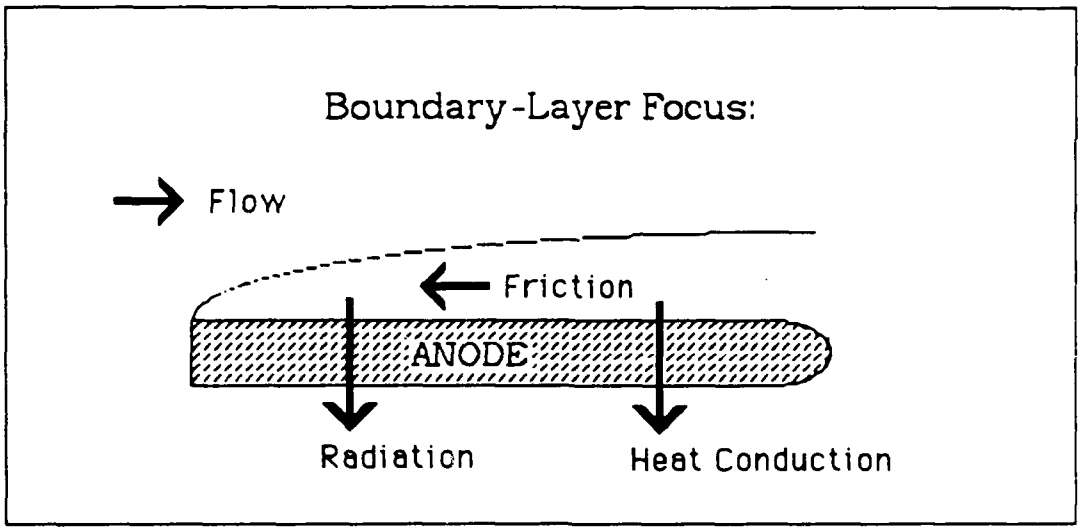

Figure 3

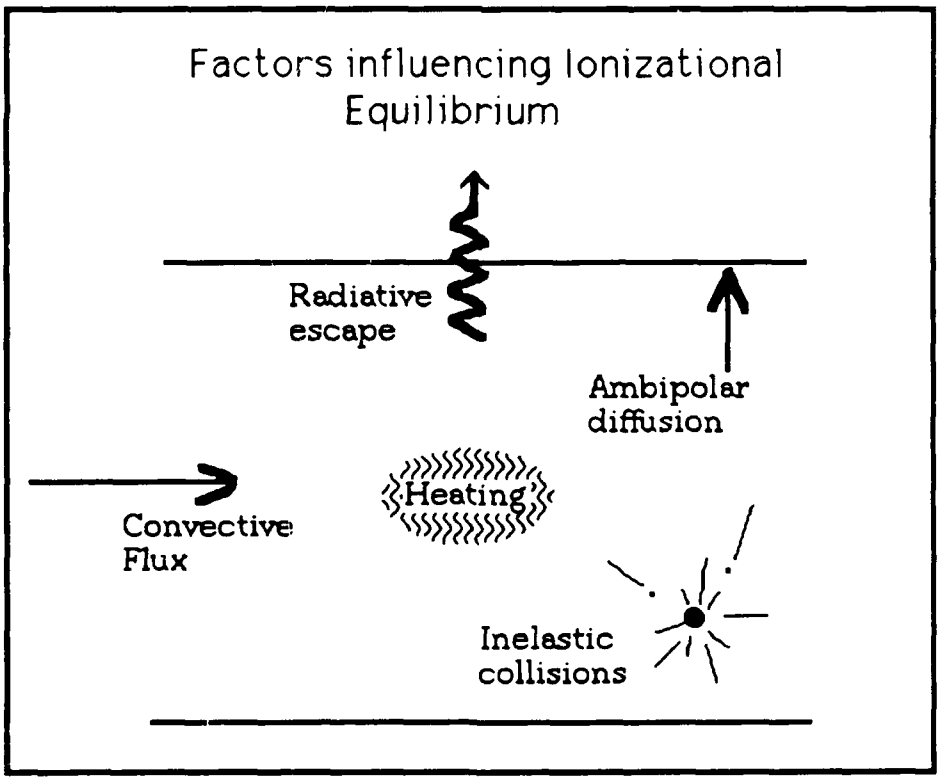

Figure 4

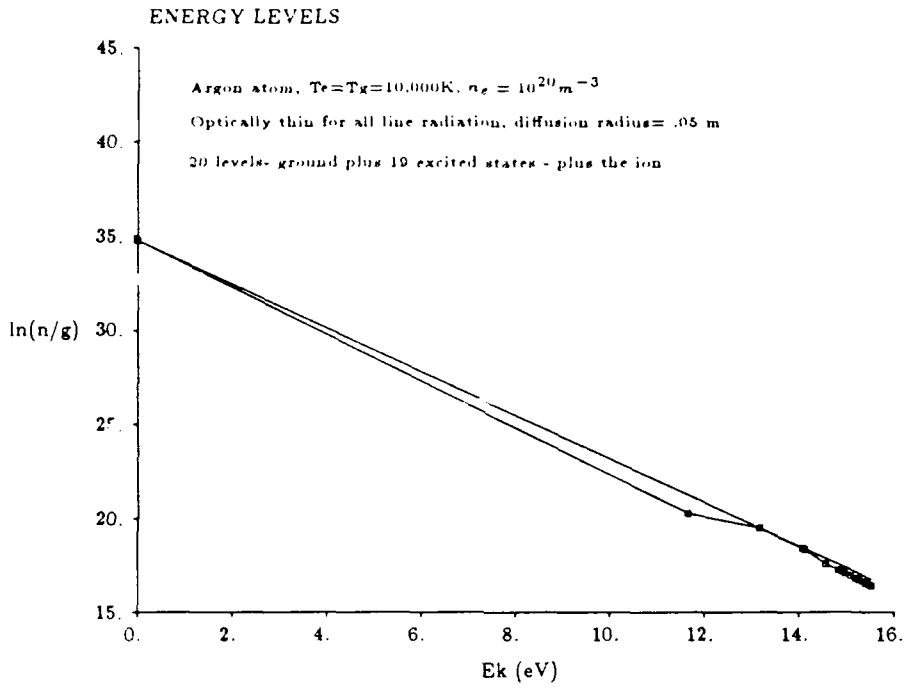

Figure 5 Boltzmann plot for the argon atom

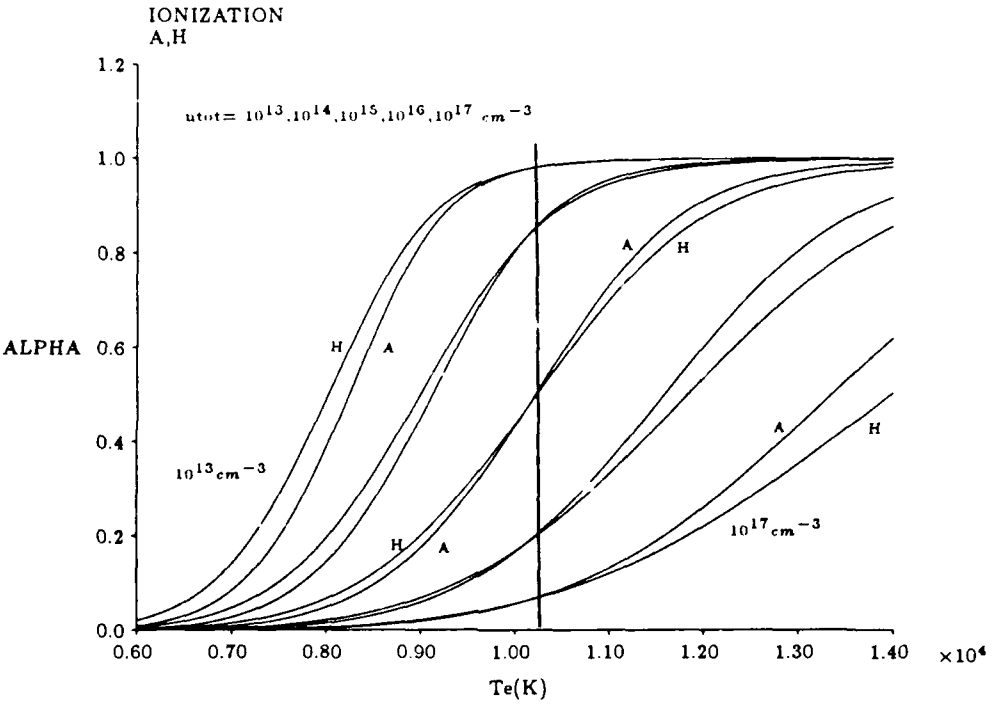

Figure 6 Crossover temperature from equilibrium ionization fraction curves

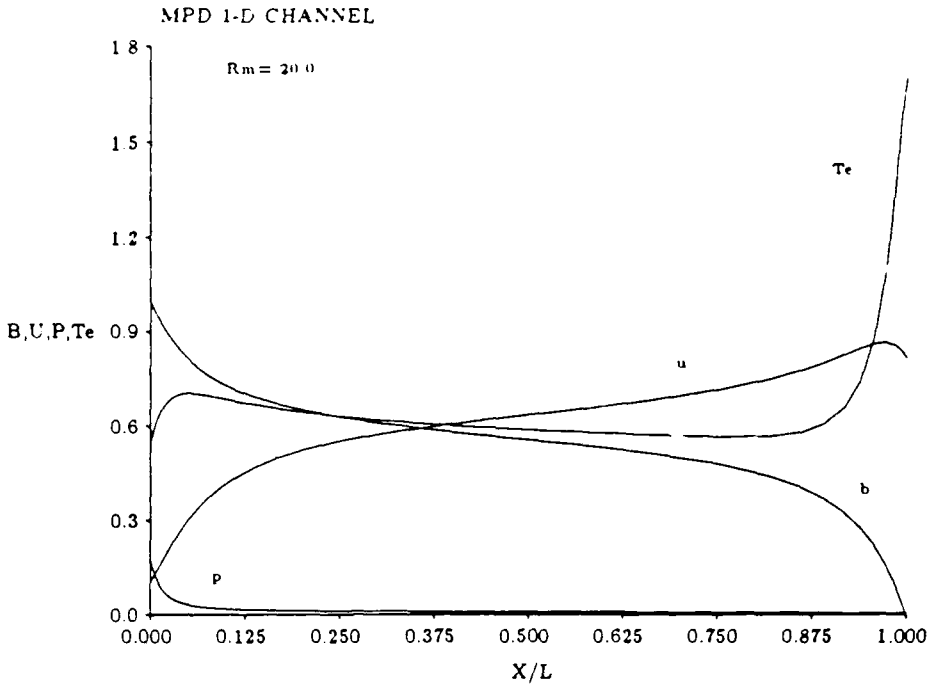

Figure 7

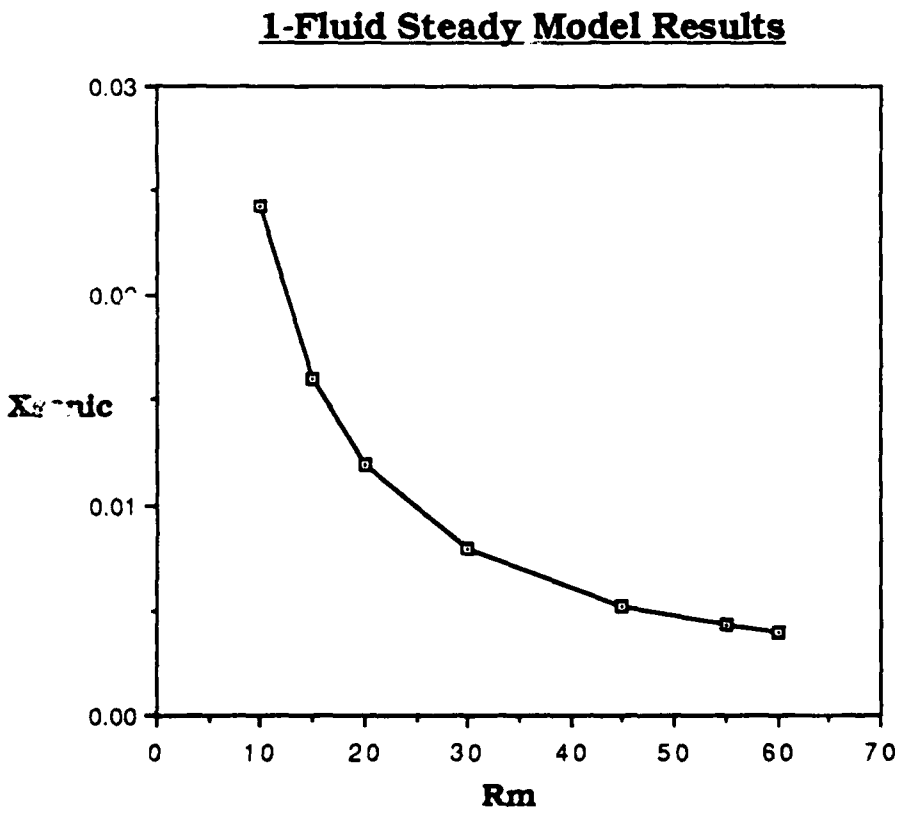

Figure 8

Two Fluid Numerical Simulations of MPD Plasmas

AFOSR GRANT-86-0019

Manuel Martinez-Sanchez

Dept of Aeronautics and Astronautics
MIT,Cambridge, MA 02139

This is a summary of work done by Eliahu Niewood, a graduate student, supported in part by the AFOSR grant.

Technical Discussion

A variety of different types of electric propulsion have been put forward as appropriate for space applications. One class of electric propulsion device is the magnetoplasmadynamic, or MPD, thruster. MPD thrusters use the Lorentz force produced by charged particles moving in an electric field to accelerate the propulsive fluid and produce thrust.

MPD channels, although simple to construct, are hard to analyze because of the complex interaction between the magnetic field and the fluid. One way to model these devices and to predict their performance is to simulate them numerically. Some numerical work has already been done with MPD thrusters. Martinez [5] and Kuriki [3] study a one fluid, fully ionized model of a steady quasi one dimensional flow. Minakuchi [6] includes the effect of axial heat conduction in his steady, one fluid, quasi one dimensional model. Subramaniam [7] and Lawless [4] worked with both the one fluid model and a partly ionized two fluid model. Heimerdinger [1] also works with a partly ionized, thermal equilibrium model, which includes viscosity. Other work has been done with two dimensional models.

This research uses a quasi one dimensional two fluid model. The model consists of fluid equations for the total density, the ionization fraction, the axial velocity, the electron temperature, and the heavy species temperature, as well as a magnetic field equation derived by combining Maxwell's equations with Ohm's law. It is assumed that all the particles have the same axial velocity, and that the ion and neutral temperatures are the same.

A number of source terms are used to model various phenomena in the flow. The electron temperature equation includes axial heat conduction. A number of source terms are used to model various phenomena in the flow. The Hinnov-Hershberg model is used to determine the ionization and recombination at each

axial location. Ambipolar diffusion is included by assuming a parabolic number density distribution across the channel. The contribution of viscosity to the momentum and the heavy species temperature equations is also included by assuming a parabolic velocity distribution. Collisional energy transfer between electrons and heavy species is also modeled. The electrical conductivity at each axial location is computed using the Spitzer-Harm formula. The viscosity and heat conduction coefficients are also computed at each axial location. All of the equations are written in their unsteady forms, and the numerical method is an unsteady method, although only steady state results have been examined so far.

The numerical method used is a combination of various schemes. This is due to the different types of equations and their different time scales. The magnetic field equation and the heat conduction term in the electron temperature equation are integrated using McCormack's method a number of times for each step of the other equations. The remaining equations are stepped using either the Donor Cell method or a modified Rusanov method.

A number of the inlet boundary conditions of the flow are determined by the physical characteristics of the flow, the mass flow per unit area, the applied current, and the total inlet enthalpy. The inlet ionization fraction is physically zero, but, because of the limitations of the model, the inlet ionization fraction is set to some small number. The inlet heavy species temperature is set to room temperature. For cases with heat conduction, the electron temperature gradient at the inlet is set to zero. For cases without heat conduction, the inlet density is computed using a downwind difference.

The exit boundary conditions for supersonic flow are zero gradient in all variables except the magnetic field, which is set to zero at the exit, and the heavy species temperature, which is chosen so that there is zero gradient in the sum of the fluid and magnetic pressures. For subsonic flow the pressure is set to some small external pressure, and the other variable are chosen so that there is zero gradient in the Riemann invariants.

The method was tested by simplifying the equations to be the unsteady analogue of the equations used by Martinez [5]. Running the simulation to steady state provided results similar to those found by Martinez for a number of different magnetic Reynolds numbers and for both constant and variable area channels.

The full set of equations were then used to examine the effect of various phenomena on the flow and performance characteristics of the thruster. The thruster was taken to be 20 cm long with an electrode seperation of 2 cm. The inlet ionization and total enthalpy were chosen to be small enough so that their effect on the flow was negligible.

First ambipolar diffusion was added to the baseline case, then viscosity, and finally, heat conduction. As shown in Table 1, ambipolar diffusion and heat conduction had little effect on performance. Viscosity however played a major role in determining thruster performance and flow characteristics. Viscosity causes

Case	R_{mag} or B_0	ambipolar diffusion	viscosity	heat conduction	channel	E_t V/m	$\tilde{T}$ N/m^2	η
1-fluid	20	no	no	no	CAC	345	4370	0.69
1-fluid	4.9258	no	no	no	CAC	433	4630	0.62
2-fluid	0.1	no	no	no	CAC	399	4256	0.57
2-fluid	0.1	yes	no	no	CAC	401	4180	0.55
2-fluid	0.1	yes	yes	no	CAC	258	2100	0.21
2-fluid	0.1	yes	yes	yes	CAC	287	2300	0.23
2-fluid	0.15	yes	yes	yes	CAC	519	4550	0.33
2-fluid	0.2	yes	yes	yes	CAC	860	6980	0.33
2-fluid	0.1	yes	yes	yes	FFC	340	3053	0.34

Table 1: Thrust and Efficiency for All Cases

the heavy species temperature to increase rapidly to levels of 1 to 10 eV and causes the flow to be frictionally choked with exit velocities on the order of 5000 meters/second .

It was also desired to determine the effect of increasing the total current supplied to the thruster, and hence the inlet magnetic field. Increasing the total current from 80 kAmp/meter-depth to 120 kA/m caused the flow to develop a large current concentration at the exit, with a corresponding increase in the exit electron temperature and ionization. Increasing the total current to 160 kA/m caused this concentration to become so large that the simulation did not converge to a steady state. As shown in Table 1, increasing the total current to 120 kA/m resulted in an increase in the thruster efficiency.

It is possible that the large exit current concentrations in the higher total current cases is due in part to the static instability described by Heimerdinger [2]. Physically this instability would first appear near the inlet and then travel down the channel. When the current buildup reaches the exit, the current would bend out of the channel and the concentration would dissipate . The current concetration would then reappear at the beginning of the channel. However, in a one dimensional model with zero exit current, the instability is forced to remain at the exit.

The last effect examined was the effect of area variation. The results for the full model at the 80 kA/m current for a constant area channel were compared to the results for a parabolic channel with an throat area of 2 cm , an inlet to throat area ratio of 1.5, and an exit to throat area ratio of 2. Area variation alleviated the exit current buildup somewhat and resulted in an increase in performance.

As detailed earlier, a model with a one dimensional magnetic field which goes to zero at the channel exit is problematic. To alleviate these problems, a two dimensional magnetic field simulation, coupled with

a quasi one dimensional fluid calculation, was developed. This simulation allows the current to bend at the exit. However, the quenching of the exit current has not yet been simulated numerically.

Some work has also been done in an attempt to combine the one dimensional MPD simulation with a model of anomalous dissipation in MPD thrusters. The dissipation arises due to the presence of a modified two stream instability in the plasma. The one dimensional code produces the parameters at each axial location needed by the dissipation model to determine if the instability exists and what its effect will be, in terms of a modified conductivity and electron and ion heating rates. The one dimensional code will then take into account the effects of the instability . By iterating this process a number of times, a steady state should be reached.

References

[1] D.J. Heimerdinger, "Fluid Mechanics in a Magnetoplasmadynamic Thruster", Doctoral Thesis, Massachusetts Institute of Technology, Jan. 1988

[2] D.J. Heimerdinger and M. Martinez Sanchez, "Fluid Mechanics in a Magnetoplasmadynamic Thruster", IEPC-88-039, DGLR/AIAA/JSASS 20th International Electric Propulsion Conference, West Germany, Oct. 1988

[3] K. Kuriki, Y. Kunii, and Y. Shimizu, "Idealized Model for Plasma Acceleration in an MHD Channel", AIAA Journal, Mar. 1983, Volume 21, Number 3

[4] J.L. Lawless and V.V. Subramaniam, "Theory of Onset in Magnetoplasmadynamic Thrusters", Journal of Propulsion and Power, Vol. 3, No. 2, Mar., Apr. 1987

[5] M. Martinez-Sanchez, "The Structure of Self Field Accelerated Plasma Flows", AIAA/DGLR/JSASS 19th International Electric Propulsion Conference, May 1987

[6] H. Minakuchi and K. Kuriki, "Magnetoplasmadynamic Analysis of Plasma Acceleration", IEPC-84-06, AIAA/DGLR/JSASS 17th International Electric Propulsion Conference

[7] V.V. Subramaniam and J.L. Lawless, "Onset in Magnetoplasmadynamic Thrusters with Finite- Rate Ionization", Journal of Propulsion and Power, Vol. 4, No. 6

Quasi One-Dimensional Numerical Simulation of Magnetoplasmadynamic Thrusters

Eliahu Haym Niewood and Prof. Manuel Martinez-Sanchez

July 19, 1989

Abstract

Magnetoplasmadynamic, or MPD, thrusters are a promising method of propulsion for a variety of different space missions. This research develops and analyzes a numerical simulation of a quasi one dimensional model for an MPD thruster. A finite difference scheme is used to integrate the fluid equations for each species and a magnetic field equation derived from Maxwell's laws. The model includes separate electron and heavy species temperatures, varying conductivity, varying ionization fraction, collisional energy transfer between heavy particles and electrons, averaged viscosity and ambipolar diffusion, and electron heat conduction. Both constant area and variable area channels are examined. The applied current in the cases studied ranges from 79.6 $\frac{kAmp}{meter\ depth}$ to 159 $\frac{kAmp}{meter\ depth}$ for an inlet mass flow of 0.5 $\frac{kg}{m^2 \cdot sec}$. It is shown that thermal equilibrium is not a valid assumption in a typical MPD thruster. It is also found that viscosity plays a significant role in determining thruster performance. Area variation is also found to have a significant effect on performance.

Nomenclature

Symbols

A Channel Area

α Ionization fraction

B Magnetic field strength

D_a Ambipolar diffusion coefficient

E_l Elastic momentum transfer between electrons and heavy species

E_i Ionization energy

e Electric charge of a proton

ϵ_o Permittivity of vacuum

Γ Spitzer logarithm

H Channel height

I Total electric current

J Electric current density

K Heat conduction coefficient

μ Viscosity coefficient

μ_0 Permeability of vacuum

n Number density

$\dot{n}_e$ Ionization rate

ν_{sr} Collision frequency of species s with species r

P Scalar fluid pressure

Q_{sr} Collision cross section of species s with species r

ρ Mass density

$S1$ Source term for continuity equation
$S2$ Source term for momentum equation
$S3$ Source term for energy equation
σ Scalar electrical conductivity
T Temperature
U Average velocity of fluid

Subscripts

$a_{s=i,e,n}$ Value of a for ion, electron, or neutral species

1 Introduction

A variety of different types of electric propulsion have been put forward as appropriate for space applications. One class of electric propulsion device is the magnetoplasmadynamic, or MPD thruster, which utilizes the Lorentz force produced by charged particles moving in a magnetic field to accelerate the propulsive fluid and produce thrust.

MPD channels, because of the interaction between the magnetic field and the fluid, are extremely complicated and hard to analyze. One possible way to understand these devices, and to predict their performance, is to simulate them numerically. Some numerical work has already been done with MPD thrusters. A number of works deal with steady quasi one dimensional flow. Martinez [14] and Kuriki [12] study a one fluid, fully ionized model. Minakuchi [17] includes the effect of heat conduction. Subramaniam [20] and Lawless [13] worked with both the one fluid model and a partly ionized two fluid model with thermal equilibrium. They include both viscosity and heat conduction to the wall in their model. Heimerdinger [7] also works with a partly ionized, thermal equilibrium model, which includes viscosity. Auweter-Kurtz [1] works with a quasi one dimensional model which allows for seperate heavy and electron temperatures, and varying ionization fraction, in parts of the thruster. Other existing works, by Chanty [2], Sleziona [19], and Park [18] examine fully two dimensional flow in both steady and unsteady cases, again with a one fluid, fully ionized model.

The model used in this research is among the first to study two fluid flow throughout the thruster with separate heavy and electron temperatures. It also includes a number of effects, such as ambipolar diffusion and collisional energy transfer, not studied previously.

2 Model

2.1 Assumptions

Due to the complexity of the problem, the model includes a number of simplifying assumptions. These are

1. The flow is quasi one dimensional.
2. Ions and neutrals are tightly coupled, so that they have equal temperatures.
3. All particles have the same average velocity in the axial direction.
4. The plasma is quasi neutral with singly ionized ions only.
5. No axial current (the Hall effect is ignored).

The working fluid in this model is Argon, with a molecular mass of $6.525 \times 10^{-26} \frac{kg}{particle}$ and an ionization energy of $2.53 \times 10^{-18} \frac{Joules}{particle}$.

2.2 Governing Equations

For a channel with varying area, where $A = HD = H \cdot$ (unit depth), the governing equations are
Global Continuity:

$$\frac{\partial \rho A}{\partial t} + \frac{\partial \rho U A}{\partial z} = 0 \tag{1}$$

Global Momentum:

$$\frac{\partial \rho U A}{\partial t} + \frac{\partial \rho U^2 A}{\partial z} + A\frac{\partial (P + \frac{B^2}{2\mu_0})}{\partial z} = AS2 \tag{2}$$

Electron Density:

$$\frac{\partial \rho \alpha A}{\partial t} + \frac{\partial \rho \alpha U A}{\partial z} = Am_i S1 \tag{3}$$

Electron Energy:

$$\frac{\partial \rho \alpha T_e A}{\partial t} + \frac{\partial \rho \alpha U T_e A}{\partial z} + \frac{2}{3}\rho \alpha T_e \frac{\partial U A}{\partial z} = A\frac{2}{3}\frac{m_i}{k} S3_e \tag{4}$$

Heavy Species Energy:

$$\frac{\partial \rho T_g A}{\partial t} + \frac{\partial \rho U T_g A}{\partial z} + \frac{2}{3}\rho T_g \frac{\partial U A}{\partial z} = A\frac{2}{3}\frac{m_i}{k} S3_g \tag{5}$$

Magnetic Field:

$$\frac{\partial BA}{\partial t} + \frac{\partial UBA}{\partial z} + \frac{1}{\sigma \mu_0}\left(\frac{A}{\sigma}\frac{\partial \sigma}{\partial z} - \frac{\partial A}{\partial z}\right)\frac{\partial B}{\partial z} = \frac{A}{\sigma \mu_0}\frac{\partial^2 B}{\partial z^2} \tag{6}$$

where, assuming Coulomb collisions are dominant, σ is given by the Spitzer-Harm formula, $\sigma = \frac{0.0153 T_e^{\frac{3}{2}}}{\ln \Gamma_e}$ in Si, and $\Gamma_e = 1.24 \times 10^7 \sqrt{\frac{T_e^3}{n_e}}$. Also, $\alpha = \frac{n_e}{n_e + n_n}$.

2.3 Source Terms

The source terms in the electron density equation represent loss and creation of electrons. One process which contributes to this source term, is the rate of ionization due to electron impact, denoted by $\dot{n}_e$. This process is evaluated using the Hinnov-Hirshberg model of ionization [15], which gives

$$\dot{n}_e = R n_e [S n_n - n_e^2] \tag{7}$$

where,

$$R = \frac{1.09 \times 10^{-20}}{T_e^{\frac{9}{2}}} \left(in \frac{m^6}{sec}\right) \tag{8}$$

and

$$S = 2.9 \times 10^{22} T_e^{\frac{3}{2}} e^{-\frac{E_i}{T_e}} \ (in\, m^{-3}) \tag{9}$$

Another process which contributes to the loss of electrons is ambipolar diffusion to the walls. Ambipolar diffusion is given by

$$\frac{\partial n_e}{\partial t} = D_a \frac{\partial^2 n_e}{\partial x^2} = \frac{12 D_a n_e}{H^2} \tag{10}$$

where D_a is the ambipolar diffusivity,

$$D_a = \sqrt{\frac{\pi k T}{4 m_i}}\left(1 + \frac{T_e}{T_g}\right)\frac{1}{Q_{in}(n_n + n_e)} \tag{11}$$

and where a parabolic distribution has been assumed for the electrons. Combining both terms yields,

$$S1 = \dot{n}_e - \frac{12 D_a n_e}{H^2} \tag{12}$$

The source term in the momentum equation comes from the viscous forces exerted on the moving fluid by the walls, so that

$$S2 = -\frac{2\mu}{H}\left(\frac{\partial U}{\partial x}\right)_w \tag{13}$$

where μ, the coefficient of viscosity is given by [16],

$$\mu = \mu_n \frac{1-\alpha}{1-\alpha+\alpha\frac{Q_{in}}{Q_{nn}}} + \mu_i \frac{\alpha}{(1-\alpha)\frac{Q_{in}}{Q_{ii}}+\alpha} \qquad (in\ \frac{kg}{m\cdot sec}) \tag{14}$$

$\mu_n = \frac{m_1 \overline{C}_1}{2Q_{nn}}$ $(in\ \frac{kg}{m\cdot sec})$ $\mu_i = \frac{0.406(4\pi\epsilon_0)^2\sqrt{m_i}(kT_g)^{\frac{3}{2}}}{e^4 \ln\Gamma_g}$ $(in\ \frac{kg}{m\cdot sec})$

$Q_{nn} = 1.7\times 10^{-18} T_g^{-\frac{1}{4}}$ $(in\ m^2)$ $Q_{in} = 1.4\times 10^{-18}$ $(in\ m^2)$ $Q_{ii} = \frac{e^4 \ln\Gamma_g}{32\pi\epsilon_0^2 k^2 T_g^2}$ $(in\ m^2)$

$\overline{C}_i = \sqrt{\frac{8kT_g}{\pi m_i}}$ $(in\ \frac{m}{s})$ $\Gamma_g = 1.24\times 10^7 \sqrt{\frac{T_g^3}{n_e}}$

A parabolic distribution is assumed for the velocity across the channel and $\frac{\partial U}{\partial x}$ is evaluated at the wall to give

$$S2 = -\frac{12 U \mu}{H^2} \tag{15}$$

One source of enery in the electron temperature equation is the Joule heating, given by $\frac{J^2}{\sigma}$. Another source of energy is collisional energy transfer between electrons and the heavy particles, denoted by E_l, where

$$E_l = 5.67\times 10^{-28}(T_e - Tg) n_e \nu_{ei} \qquad (in\ \frac{watts}{m^3}) \tag{16}$$

where,

$\nu_{ei} = \frac{\overline{C}_e n_e Q_{ei}}{1.98}$ $(in\ \frac{1}{s})$ $Q_{ei} = \frac{5.85\times 10^{-10} ln\Gamma_e}{T_e^2}$ $(in\ m^2)$ $\overline{C}_e = 6214.0\sqrt{T_e}$ $(in\ \frac{m}{sec})$

Since the internal energy as defined does not include the ionization energy of the electrons, energy is also lost when an electron ionizes, so there is a loss equal to $E_i \dot{n}_e$. Also included in this source term is the axial heat conduction, given by $\frac{\partial}{\partial z}(K_e \frac{\partial T_e}{\partial z})$, where [15],

$$K_e = \frac{1.7142 k^2 T_e \sigma}{e^2} \qquad (in \frac{watt}{m\cdot K}) \tag{17}$$

Radial heat conduction to the electrodes is assumed to be small due to the confining effect of the sheath, although this asssumption needs to be examined in more depth. Including all of these processes,

$$S3_e = \frac{J^2}{\sigma} - E_l - E_i \dot{n}_e + \frac{\partial}{\partial z}(K_e \frac{\partial T_e}{\partial z}) \tag{18}$$

The source term for the heavy particle temperature equation includes the energy lost to the electrons, described earlier, and the heat produced by the viscous force applied by the wall to the fluid. This heat is given by $\mu(\frac{\partial U}{\partial x})^2$, which is averaged over the channel again assuming a parabolic velocity distribution. Therefore,

$$S3_g = E_l + \frac{12 U^2 \mu}{H^2} \tag{19}$$

3 Numerical Method

3.1 Overall Scheme

The overall numerical scheme is as follows:

1. Evaluate all of the source terms.
2. Integrate the magnetic field equation the neccessary number of times, holding all other variables constant. The magnetic field integration is done using McCormack's method.
3. Integrate the convective terms of the fluid equations using a modification of Rusanov's method, for the overall density and momentum equations and the Donor Cell method for the electron density and species temperature equations.
4. Add in the contribution from the source terms.
5. Integrate the diffusive part of the electron temperature equation, again using McCormack's method.

3.2 Inlet Boundary Conditions

The mass flow per unit area was chosen to be 0.5 $\frac{kg}{m^2 \cdot s}$ in all cases. The magnetic field at the inlet is determined by the total applied current I, assumed to be constant, $B_0 = \frac{\mu_0 I}{D}$. The inlet ionization fraction is assumed to be constant and small, equal to 0.01. The inlet density is found by a downwind difference, a one sided finite difference formulation of the overall continuity equation at the zeroth point. The total inlet enthalpy is assumed to be $2.1 \times 10^5 \frac{m^2}{s^2}$ in the one fluid test cases, equivalent to the enthalpy of a room temperature gas, and $5.5 \times 10^5 \frac{m^2}{s^2}$ in the two fluid cases, to allow for the inlet ionization.

For cases without electron heat conduction the heavy species temperature at the inlet is assumed to be constant and equal to room temperature, 300 K. The electron temperature is then found as a function of the known variables and the total inlet enthalpy. For cases with electron heat conduction, the electron temperature is assumed to be the same as that at the next inside point, and the gas temperature is then found as a function of the other known quantities.

3.3 Outlet Boundary Conditions

At the outlet it is assumed that if the flow is supersonic, the variables at the exit are set equal to the variables at the closest inside point with the exception of the magnetic field, which is set to zero. If the flow is subsonic, the fluid variables ρ and U are given by the Riemann invariants, while P is determined by the external pressure, assumed to be some very small pressure. The electron temperature and ionization fraction are again taken from the inside point and the heavy species temperature is then computed as in the supersonic case.

4 Results

4.1 One Fluid Results

It is possible to solve the one fluid equations with the method developed for the two fluid equations. The one fluid case therefore served as a valuable test for the method, because it has already been analyzed by others. Martinez [14] uses a space marching method with an inner-outer expansion to find the steady state solution to the one fluid equationsand examines the nature of the $R_m \rightarrow \infty$ limit

Interelectrode Separation: 2 cm	$\frac{\dot{m}}{A^*} = 0.5 \frac{kg}{m^2 \cdot sec}$
Channel Length = 20 cm	$B_0 = 0.1$ Tesla
$T_0 = 300$ K	$I = 79.6 \frac{kAmp}{m \cdot depth}$

Table 1: Thruster Characteristics

by means of inner-outer expansions at the inlet and the exit. A test case was run using the thruster described in Table 1. The electric field calculated for the test case was within 2% of that calculated by Martinez.

4.2 Comparison of Two Fluid and One Fluid Results

After the one fluid results had been obtained and verified, the equivalent two fluid case was run to allow comparisons of the one fluid and two fluid models. This case did not include ambipolar diffusion, viscosity or heat conduction, as these effects are not included in the one fluid model. One important feature of these results, labeled Case 1 in Figures 1 - 4, is the large discrepancy between the electron and heavy species temperatures. The heavy species temperature is an order of magnitude smaller than the electron temperature. This would imply that the thermal equilibrium assumed by the one fluid model is not a good assumption. This large difference in temperature arises because there is no effective mechanism in the model of Case 1 for heating the heavy species. The only source term in the heavy species temperature equation, collisional energy transfer with the electrons, is a relatively weak effect. The difference in temperatures also means that any electrical or thermal conductivities or viscosity coefficients computed on the basis of some combined temperature will be inaccurate.

A two fluid model is also neccessary for evaluating the importance and effect of plasma instabilities, such as those discussed by Choueri [3], [4] and Hastings [6]. These instabilities are often dependent on the individual species temperatures.

4.3 Effect of Viscosity

Three more cases were then run, adding one effect in each case. The first addition that was made was ambipolar diffusion. The results for this case are labeled Case 2. The addition of ambipolar diffusion has caused a sharp decrease in the ionization fraction, and a smaller decrease in the gas temperature. The electron temperature has increased to compensate for the diffusion loss in the ionization fraction. However, ambipolar diffusion has little effect on the thruster performance as given in Table 5 . This seems to be because the electrons and ions which are now being lost to the side walls were lost at the channel exit in Case 1. Although the electrodes will be heated by the diffusing particles, electrode temperature is not included in the model. However, as shown in Table 3 for Case 4, ambipolar loss absorbs a substantial fraction of the dissipation, so that there will be a great deal of electrode heating.

Recent work by Kilfoyle [10] and Kuriki [11] both show measured gas temperatures which equal and even exceed the electron temperatures. Kilfoyle finds T_g ranging from 1eV up to 7eV, or up to 80,000K. Kuriki finds heavy particle temperatures of up to 70,000K. As shown in Figure 3, the inviscid model predicts gas temperatures of only 5000K. Some additional source must be adding energy to the heavy species. Heimerdinger et al. [8] and Kilfoyle [10] propose viscous dissipation as this source. Therefore, the second effect examined was the addition of viscosity to the model. The results using this model are labeled Case 3. As can be seen in these figures, the heavy species temperature increases to the levels found experimentally. This would seem to justify the hypothesis that viscous effects could cause high heavy species temperatures. The higher temperature leads to higher pressure throughout the channel. Also, the flow now seems to be frictionally choked, so that the velocity levels off toward the beginning

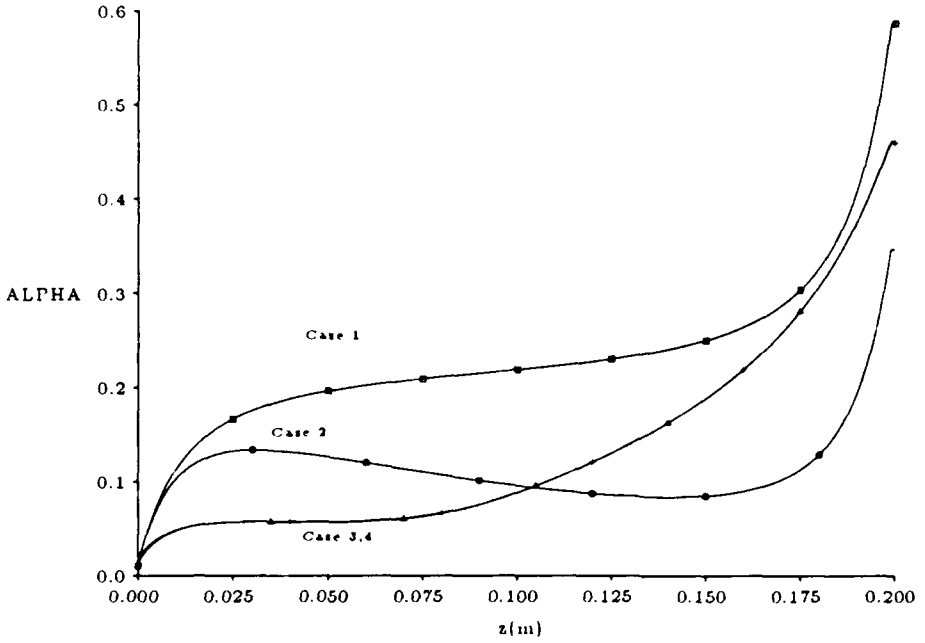

Figure 1: Two Fluid Results: *Ionization Fraction*

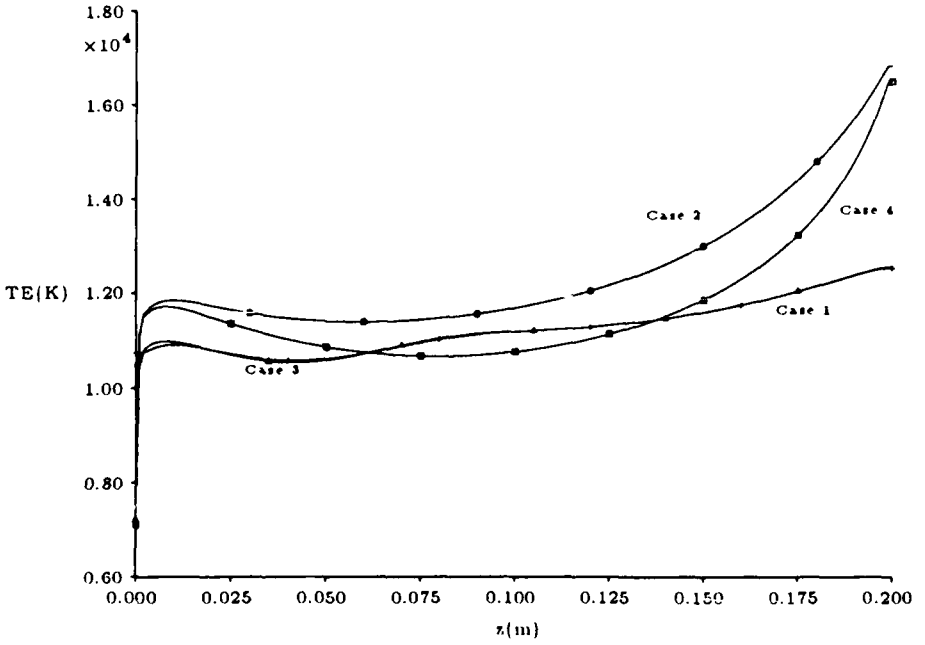

Figure 2: Two Fluid Results: Electron Temperature

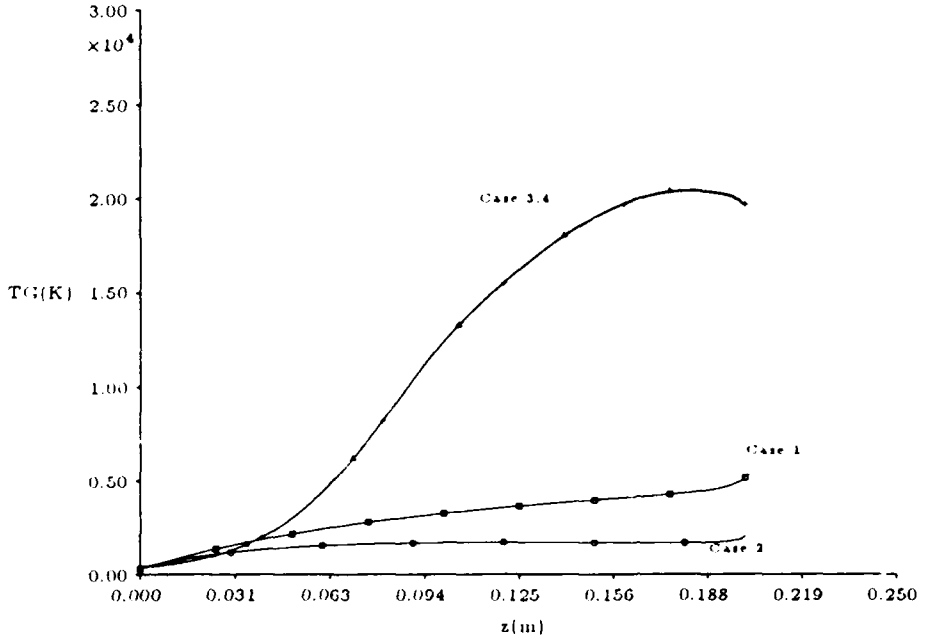

Figure 3: Two Fluid Results: Heavy Species Temperature

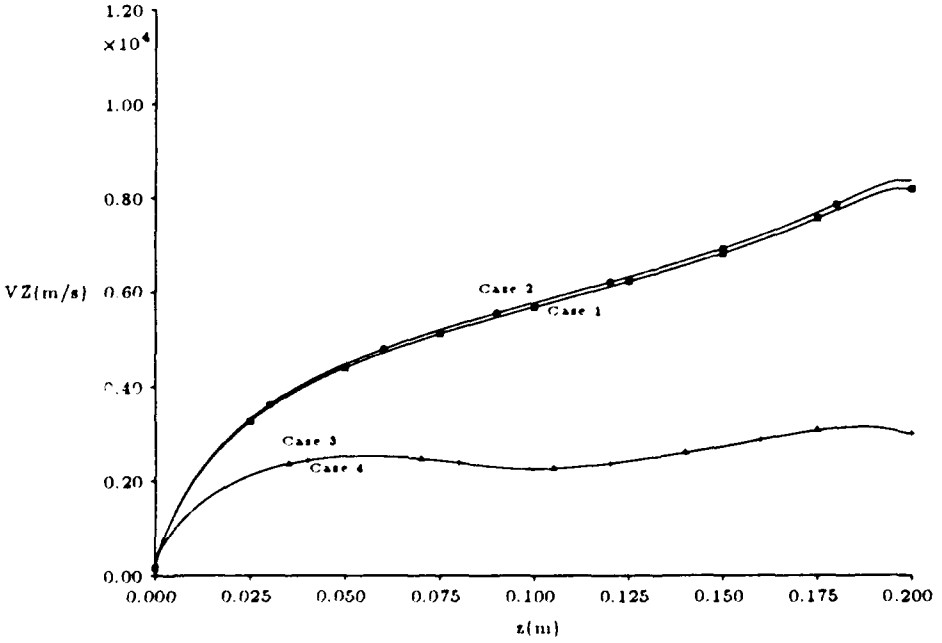

Figure 4: Two Fluid Results: Velocity

Z(cm)	ionization	recombination	ambipolar diffusion
0.5	1.11	0.26	0.91
2.5	0.68	0.09	0.80
4.5	1.08	0.08	0.78
6.5	1.71	0.10	0.85
8.5	2.25	0.12	1.01
10.5	2.83	0.16	1.22
12.5	3.56	0.20	1.50
14.5	4.58	0.25	1.86
16.5	6.30	0.34	2.37
18.5	9.93	0.56	3.17

Table 2: Magnitude of Terms in the Ionization Fraction Equation

of the channel, and does not increase to the levels found in Cases 1 and 2. As shown in Table 5 the thrust and the efficiency have both dropped considerably, .

Heimerdinger [7] also included viscosity, but assumed thermal equilibrium. He also computed the ionization fraction by balancing recombination with local ionization. His results show an ionization fraction which varies almost linearly with z. This is in part due to the large variation in the overall temperature which is used to compute the ionization. By separating the electron and heavy species temperatures, this research finds a lower ionization fraction in the bulk of the channel with the ionization fraction increasing sharply at the exit. The variation of the viscosity coefficient and the velocity distribution are also quite different than in Heimerdinger.

One other process which was added to the model was electron axial heat conduction. The results for this case are labeled Case 4. The results for this case are quite similar to those of Case 3. The thrust and efficiency for this case are again shown in Table 5.

4.4 Relative Importance of Effects

In steady state, the ionization fraction equation becomes

$$\frac{\partial \alpha}{\partial z} = \frac{A}{\dot{m}} m_i R n_e S n_n - \frac{A}{\dot{m}} m_i R n_e^3 - \frac{A}{\dot{m}} m_i \frac{12 D_a n_e}{H^2} \tag{20}$$

For Case 4, the complete model, the relative magnitude of each of these effects at various locations in the channel is given in Table 2. It is seen that recombination is a relatively weak effect. At the beginning of the channel, ambipolar diffusion and ionization are almost equal. However, as the electron temperature increases, ionization becomes almost twice as large as ambipolar diffusion. The electron energy equation can also be broken down in this way. Again, in steady state,

$$\frac{E_i}{k}\frac{\partial \alpha}{\partial z} + \frac{3}{2} T_e \frac{\partial \alpha}{\partial z} + \frac{3}{2}\alpha \frac{\partial T_e}{\partial z} - \frac{\alpha T_e}{\rho}\frac{\partial \rho}{\partial z} =$$

$$\frac{m_i}{k\rho U}\frac{J^2}{\sigma} - \frac{m_i}{k\rho U} E_l - \frac{m_i}{k\rho U}\frac{\partial}{\partial z}\left(K_e \frac{\partial T_e}{\partial z}\right) - \frac{m_i}{k\rho U} E_i 12 D_a \frac{n_e}{H^2}$$

In words, Ionization Energy + Temperature Energy + Electron Heating - Pressure Work = Dissipation - Collisional Transfer - Heat Conduction - Ambipolar Loss. The relative magnitude of each of these terms is given in Table 3. For the most part, dissipation is balanced by ionization energy and ambipolar loss, although collisional energy transfer is also a significant term, particularly near the inlet. Notice

Z(cm)	Ionization Energy	Temper. Energy	Electron Heating	Pressure Work	Dissi-pation	Collisional Transfer	Heat Cond.	Ambipolar Loss
0.5	0.59	0.05	0.03	-0.21	3.66	1.37	-0.37	1.67
2.5	-0.32	-0.03	0.02	-0.02	1.60	0.52	-0.16	1.46
4.5	0.46	0.04	0.03	0.01	2.12	0.22	-0.26	1.41
6.5	1.40	0.12	0.02	-0.01	3.02	-0.09	-0.16	1.56
8.5	2.05	0.18	0.02	-0.02	3.64	-0.48	-0.15	1.84
10.5	2.65	0.24	0.02	-0.03	4.27	-0.96	-0.17	2.24
12.5	3.39	0.31	0.03	-0.05	5.11	-1.47	-0.21	2.75
14.5	4.53	0.42	0.05	-0.07	6.53	-2.0	-0.28	3.42
16.5	6.65	0.64	0.08	-0.07	9.21	-2 56	-0.39	4.34
18.5	11.68	1.16	0.13	0.0	15.04	-3.40	-0.51	5.81

Table 3: Magnitude of Terms in the Electron Energy Equation, $\times 10^{-5}$

also that near the exit the ions are actually significantly heating the electrons. Heat conduction and electron heating play a small role, while pressure work is negligible.

5 Area Variation

Using the full model of Case 4, the flow in the constant area channel was compared to the flow in a converging-diverging, or fully flared, channel (FFC). The interelectrode separation for the channel is shown in Figure 5. The flow is compared to that in a constant area channel (CAC) in Figures 6 - 8.

The channels examined were chosen to be similar to those examined experimentaly by Heimerdinger, Kilfoyle, and Martinez [7], and have the same length, the same throat area, and the same inlet and exit area ratios. Heimerdinger proposes area variation as a means of reducing inlet and exit current concentrations. This is seen to be the case, particularly at the exit.

As given in Table 5, there is a significant increase in performance for the variable area channel. This is in part due to a decrease in the effect of viscosity on the velocity, as the viscous source term in the momentum equation varies as $\frac{U}{H^2}$ Since H has increased, the magnitude of this term has dropped, despite the increase in U. One other difference with the constant area channel is the higher electron temperature in the fully flared channel. This can be explained by examining Table 4 which gives the magnitude of the terms in the electron energy equation. Comparing this table to Table 3 points out a number of differences between the two channels. First, collisional energy transfer at the ends of the FFC is around 50% of its value at the ends of the CAC. This is because collisional energy transfer scales with density, which is smaller at the ends of the FFC, because of the increased area. Ambipolar loss is also smaller at the ends of the FFC, because of the increased interelectrode distance. In the center of the channel, where both of these effects are of the same magnitude as in the CAC, the increased throat dissipation of the FFC keeps the electron temperature higher than in the CAC.

6 Performance

The thrust and efficiency for the various cases are shown in Table 5. There are a number of loss mechanisms that prevent the thruster from being 100% efficient. One reason for the decreased efficiency is the frozen flow losses. Since the residence time of the fluid in the channel is short, the composition of the fluid is not the equilibrium composition. Therefore, some of the energy used to ionize the neutral fluid is not recovered. Ambipolar diffusion, although it changes where losses occur, does not seem to

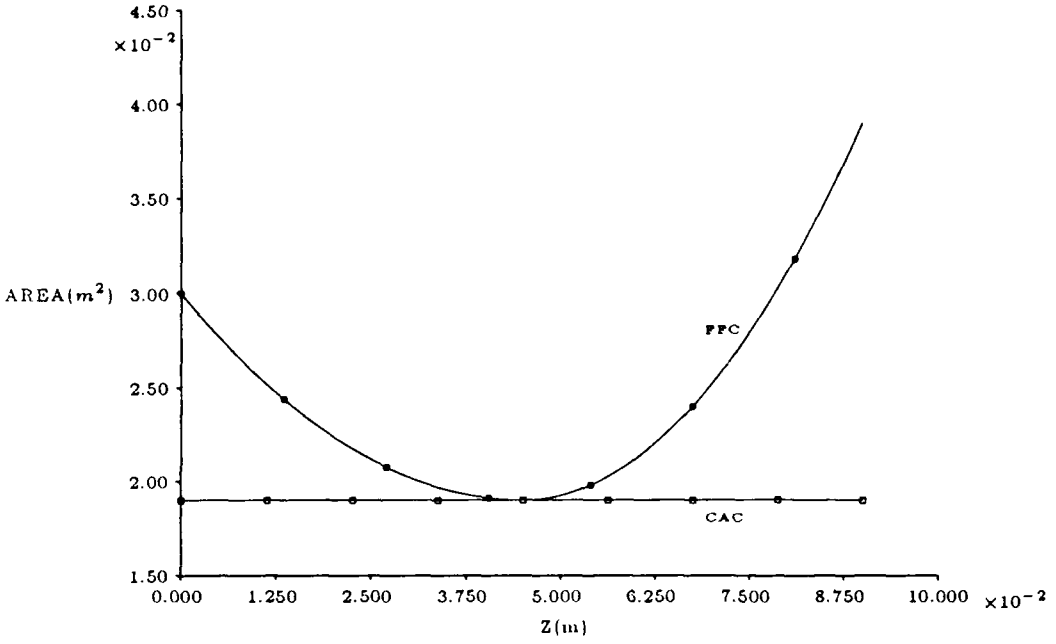

Figure 5: Inter-Electrode Separation of Fully Flared and Constant Area Channels

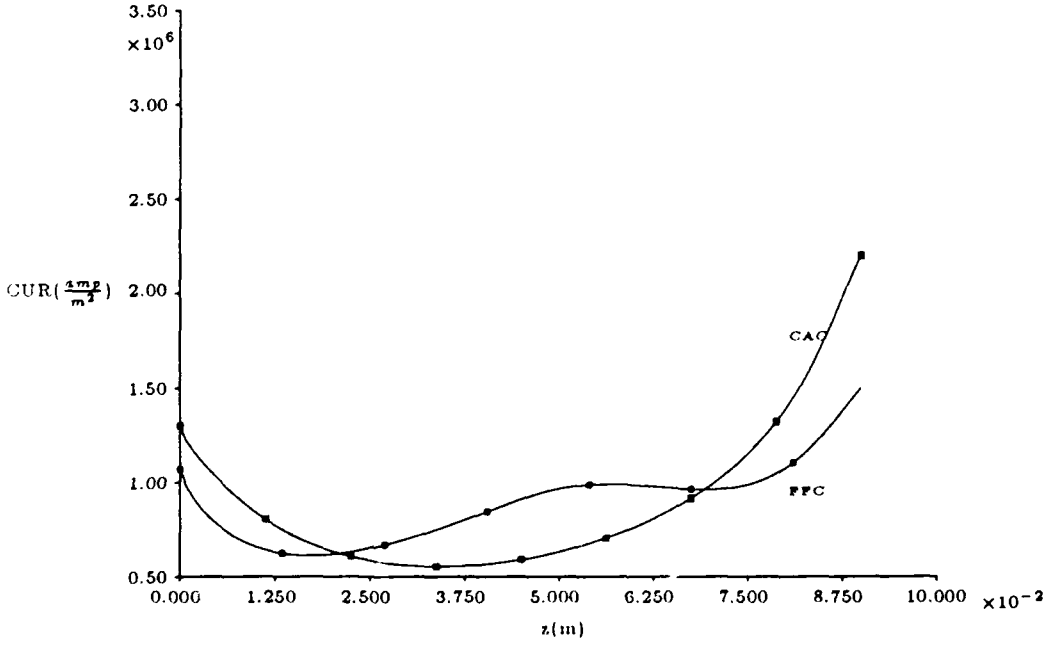

Figure 6: Fully Flared and Constant Area Channels: Current Density

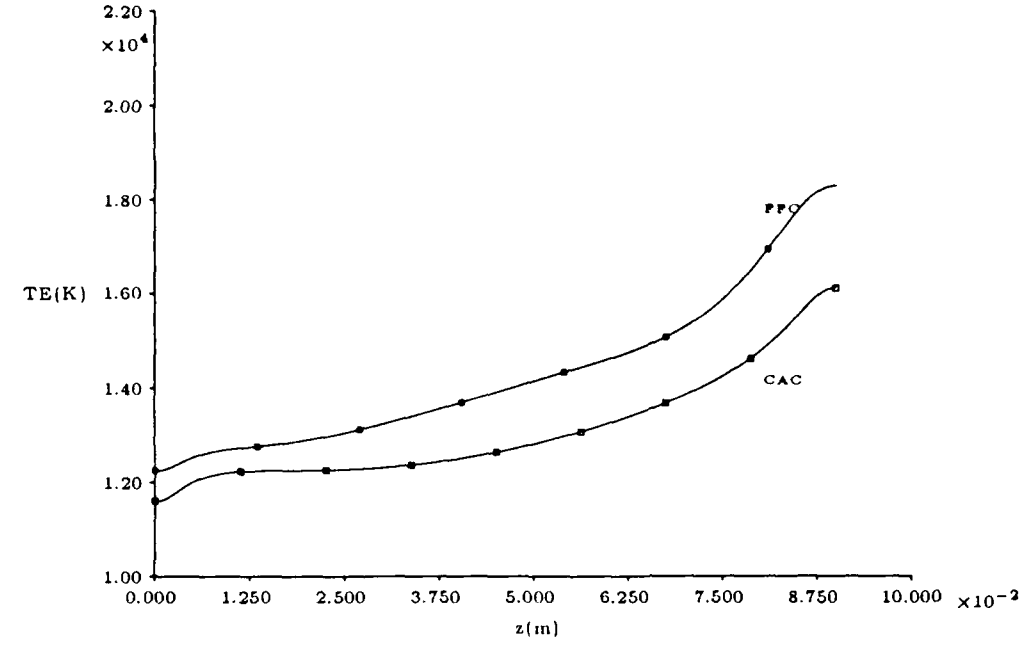

Figure 7: Fully Flared and Constant Area Channels: Electron Temperature

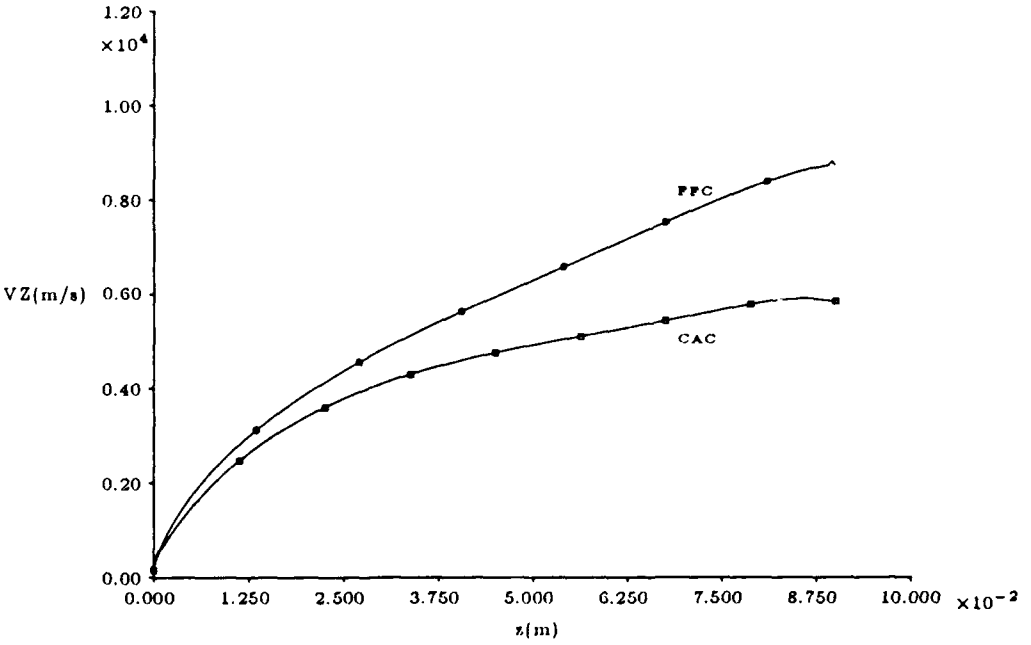

Figure 8: Fully Flared and Constant Area Channels: Velocity

Z(cm)	Ionization Energy	Temper. Energy	Electron Heating	Pressure Work	Dissi-pation	Collisional Transfer	Heat Cond.	Ambipolar Loss
0.5	2.48	0.22	0.0	-0.17	4.32	0.50	-0.09	0.94
2.5	0.19	0.02	0.01	-0.02	1.34	0.23	-0.09	0.96
4.5	0.78	0.07	0.03	0.01	1.90	0.16	-0.46	0.93
6.5	2.70	0.25	0.02	0.02	4.16	0.10	-0.33	1.17
8.5	4.82	0.46	0.01	-0.03	6.97	-0.22	-0.14	1.83
10.5	5.56	0.53	0.03	-0.10	8.31	-0.83	-0.22	2.74
12.5	5.24	0.51	0.04	-0.18	8.43	-1.29	-0.28	3.48
14.5	4.75	0.48	0.07	-0.25	8.24	-1.43	-0.39	3.81
16.5	5.04	0.52	0.12	-0.32	8.81	-1.31	-0.77	3.84
18.5	7.83	0.85	0.28	-0.36	12.15	-1.10	-1.97	3.83

Table 4: Magnitude of Terms in the Electron Energy Equation, $\times 10^{-5}$

Case	B_0	ambipolar diffusion	viscosity	heat conduction	channel	E_t V/m	$\bar{T}$ N/m^2	η
1-fluid	0.1	no	no	no	CAC,20cm	433	4630	0.62
2-fluid	0.1	no	no	no	CAC,20cm	399	4256	0.57
2-fluid	0.1	yes	no	no	CAC,20cm	401	4180	0.55
2-fluid	0.1	yes	yes	no	CAC,20cm	258	2100	0.21
2-fluid	0.1	yes	yes	yes	CAC,20cm	287	2300	0.23
2-fluid	0.1	yes	yes	yes	CAC,9cm	469	3535	0.34
2-fluid	0.1	yes	yes	yes	FFC,9cm	600	4717	0.47

Table 5: Thrust and Efficiency for All Cases

change the amount of loss. However, adding viscosity to the model does cause a large drop in efficiency. At the low inlet magnetic field, heat conduction does not affect the efficiency significantly.

7 Conclusions

This research had a number of goals. The first was to develop a numerical method with which to analyze a two fluid model. That goal has been achieved, and it has been shown that there are some significant differences between the one fluid and the two fluid results. The method developed has proven to be very versatile, and should become a useful tool in thruster analysis. Also, the method has been tested against previous one fluid work and has been shown to be accurate. A second goal was to determine the effect of viscosity on the thruster fluid flow. It has been seen that viscosity raises the gas temperature to levels found experimentally. The relative importance of various effects on the flow has also been calculated. Finally, area variation has been shown to increase efficiency by a significant amount, and reduce exit current concentrations.

Acknowledgements

This material is based upon work supported under a National Science Foundation Graduate Fellowship.

References

[1] M. Auweter-Kurtz, H.L. Kurtz, H.O. Schrade, and P.C. Sleziona, "Numerical Modeling of the Flow Discharge in MPD Thrusters", Journal of Propulsion and Power, Vol. 5, No. 1, Jan.-Feb. 1989

[2] J.M.G. Chanty and M. Martinez-Sanchez, "Two-Dimensional Numerical Simulation of MPD Flows", AIAA-87-1090, AIAA/DGLR/JSASS 19th International Electric Propulsion Conference, Colorado, May 1987

[3] E.Y. Choueiri, A.J. Kelly, and R.G. Jahn, "MPD Thruster Plasma Instability Studies", AIAA-87-1067, AIAA/JSASS/DGLR 19th International Electric Propulsion Conference, Colorado, May 1987

[4] E.Y. Choueiri, A.J. Kelly, and R.G. Jahn, "Current Driven Instabilities of an Electromagnetically Accelerated Plasma", DGLR/AIAA/ JSASS 20th International Electric Propulsion Conference, W. Germany, Oct. 1988

[5] M.S. Di Capua and R.G. Jahn, "Energy Deposition in Parallel-Plate Plasma Accelerators", AIAA 9th Aerospace Sciences Meeting, New York, Jan. 1971

[6] D.E. Hastings and E.H. Niewood, "Theory of the Modified Two Stream Instability in an MPD thruster", submitted to the Journal of Propulsion and Power

[7] D.J. Heimerdinger, "Fluid Mechanics in a Magnetoplasmadynamic Thruster", Doctoral Thesis, Massachusetts Institute of Technology, Jan. 1988

[8] D.J. Heimerdinger, D.B. Kilfoyle, and M. Martinez-Sanchez, "Experimental Characterization of Contoured Magnetoplasmadynamic Thrusters", AIAA-88-3205 AIAA/ASME/SAE/ASEE 24th Joint Propulsion Conference, Boston, July 1988

[9] D.J. Heimerdinger and M. Martinez-Sanchez, "Fluid Mechanics in a Magnetoplasmadynamic Thruster", IEPC-88-039, DGLR/AIAA/JSASS 20th International Electric Propulsion Conference, West Germany, Oct. 1988

[10] D.B. Kilfoyle, M. Martinez-Sanchez, D.J. Heimerdinger, and E.J. Sheppard, "Spectroscopic Investigation of the Exit Plane of an MPD Thruster", IEPC-88-027, DGLR/AIAA/JSASS 20th International Electric Propulsion Conference, West Germany, Oct. 1988

[11] Y. Kunii, "Multipole MPD Arcjet", AIAA-85-2055, AIAA/DGLR/JSASS 18th International Electric Propulsion Conference, Virginia, Sept. 1985

[12] K. Kuriki, Y. Kunii, and Y. Shimizu, "Idealized Model for Plasma Acceleration in an MHD Channel", AIAA Journal, Mar. 1983, Volume 21, Number 3

[13] J.L. Lawless and V.V. Subramaniam, "Theory of Onset in Magnetoplasmadynamic Thrusters", Journal of Propulsion and Power, Vol. 3, No. 2, Mar. Apr. 1987

[14] M. Martinez Sanchez, "Structure of Self Field Accelerated Plasma Flows", AIAA/DGLR/JSASS 19th International Electric Propulsion Conference, May 1987

[15] M. Mitchner and C. Kruger, *Partially Ionized Gases*, John Wiley and Sons, New York, 1973

[16] Scott Miller, SM Candidate, Dept. of Aeronautics and Astronautics, M.I.T., private communication

[17] H. Minakuchi and K. Kuriki, "Magnetoplasmadynamic Analysis of Plasma Acceleration", IEPC-84-06, AIAA/DGLR/JSASS 17th International Electric Propulsion Conference

[18] Won-Taek Park and Duk-in Choi, "Two Dimensional Model of the Plasma Thruster", Journal of Propulsion and Power, Mar. Apr. 1988, Volume 4, Number 2

[19] P.C. Sleziona, Auweter-Kurtz, M. and H.O. Schrade," Numerical Codes for Cylindrical MPD Thrusters, 88-038, DGLR/AIAA/JSASS 20th International Electric Propulsion Conference", West Germany, Oct. 1988

[20] V.V. Subramaniam and J.L. Lawless, "Onset in Magnetoplasmadynamic Thrusters with Finite-Rate Ionization", Journal of Propulsion and Power, Vol. 4, No. 6

AIAA-87-1090
Two-Dimensional Numerical Simulation of MPD Flows

J. M. G. Chanty and M. Martinez-Sanchez,
Massachusetts Institute of Technology,
Cambridge, MA

AIAA/DGLR/JSASS 19th International Electric Propulsion Conference
May 11-13,1987
Colorado Springs, Colorado

AIAA-87-1090

Two-Dimensional Numerical Simulation of MPD Flows

J. M. G. Chanty*, M. Martinez-Sanchez†

Space Systems Laboratory, Department of Aeronautics and Astronautics

Massachusets Institute of Technology, Cambridge, MA. 02139

Abstract

A two-dimensional numerical model has been developed in order to analyze electro-magnetic plasma accelerators also called Self-Field Magneto-Plasma-Dynamic Thrusters. This model uses a Magneto-Hydro-Dynamic description of the gas considered as a fully ionized, isothermal plasma, and takes into account the Hall effect (non linear conductivity) and the interaction between the magnetic field and the fluid dynamics of the plasma. The system of equations is discretized into finite volumes, and is solved by a Newton-Raphson scheme. Results from the MHD model were calculated for a mass flow rate of 6 g/s of Argon and for currents up to ten kilo-Amperes.

Introduction

During the past years the development of high current plasma accelerators (also called Magneto-Plasma-Dynamic Thrusters) has been aimed, among other things, at improving the efficiency of energy conversion from electrical to kinetic energy. Several researchers have observed that the efficiency increases with the current, but at some value a transition occurs to an unstable and destructive regime of the discharge (called onset of instability in the literature), when the ratio $\frac{I^2}{\dot{m}}$ exceeds a critical value which depends on the nature of the propellant and the thruster geometry. Some researchers [3] [11] have proposed a theory for the transition to an unstable behavior based on the depletion of the anode from current-carrying electrons, the formation of a starvation layer along the anode characterized by current densities in excess of the random thermal flux of electrons, and the reversing of the potential drop between the the plasma and the electrode. In order to study the formation of this starvation layer one needs to take the geometrical properties of the discharge into account, or in other words, to look at a two-dimensional model of the discharge. Eventually this model can be used to find optimal shapes that maximise certain parameters like efficiency or electrode life.

Various attempts have been made to develop numerical two-dimensional models of MPD discharges using finite element or finite difference descriptions. I. Kimura *et al.* [17] have presented a two dimensional model for the electromagnetic field (self field), including the Hall effect. The model was primarily designed to calculate the current distribution near the cathode. They later extended their model [27] to systems that work with an external focussing magnetic field. These models, however, were not designed for an accurate modelling of realistic thruster geometries, and did not include the effect of the convection of the electromagnetic field by the plasma. This last limitation was partially removed in a later paper [28] where a simplified calculation of the flow was made and coupled with the magnetic field. Ao and Fujiwara [1] have attempted to develop a one-fluid Magneto-Hydro-Dynamic model of the plasma where the equations describing the motion of the plasma, considered as a neutral conductive fluid, are coupled with the magnetic field through the Lorentz force and the ohmic heating. However this model was limited to a very simple geometry.

It was decided to develop a two-dimensional numerical model based on a MHD description of the plasma in the collision dominated regime, in order to calculate the steady state distribution of the electro-magnetic field and the motion of the plasma in the accelerator. We focused our attention on the phenomena observed at the electrodes, especially at the anode, in an effort to detect the onset of the turbulent regime.

The system of partial differential equations is discretized using a finite volume technique used extensively in Computational Fluid Dynamic algorithms. The system of equations was solved using a Newton-Raphson method, derived from an initial calculation of the magnetic field alone for which this method works well due to the dominant elliptic behavior of the equations. The method of discretization of the equations (finite volume method) as well as the idea of the addition of an artificial viscosity. was derived from Jameson and Yoon [15]. A confirmation of the possibility of the Newton-Raphson method was found in the lecture of Jespersen [16], as well as in the doctoral theses of M. Giles [8] and M. Drela [7]

*Graduate Student

†Associate Professor

Physical Model

The equations describing the model are derived from the general Magneto-Hydro-Dynamic approximation which includes the following equations: conservation of mass, momentum and energy in the inviscid fluid; the Ohm's law (derived from the electron momentum conservation); and the quasi-static Maxwell's equations.

$$\partial_t \rho + \nabla(\rho \mathbf{u}) = 0$$

$$\partial_t \rho \mathbf{u} + \mathrm{Div}(\rho \overline{\overline{\mathbf{uu}}} - \overline{\overline{\mathbf{S}}} - \overline{\overline{\mathbf{M}}}) = 0$$

Where $\overline{\overline{S}}$ is the pressure stress tensor, and $\overline{\overline{M}}$ is the Maxwell stress tensor.

$$\partial_t(E_{EM} + E_I + E_K) + \nabla \cdot ((E_I + E_K + P)\mathbf{u} + \frac{\mathbf{E} \times \mathbf{B}}{\mu_0} + \mathbf{q}) = 0$$

Where E_{EM}, E_I, E_K are respectively the electromagnetic energy ($B^2/2\mu_0$), the internal energy, and the kinetic energy, per unit volume; P is the pressure; $\frac{\mathbf{E} \times \mathbf{B}}{\mu_0}$ is the Poynting vector; $\mathbf{q}$ is the heat conduction. The energy-equation is usually completed by a state equation relating the pressure to the internal energy, for instance :

$$P = (\gamma - 1)E_I$$

The generalized Ohm's law can be written as:

$$\mathbf{E} + \mathbf{u} \times \mathbf{B} = \frac{1}{\sigma}\mathbf{J} + \frac{1}{en_e}\mathbf{J} \times \mathbf{B} - \frac{\nabla P_e}{en_e}$$

The Maxwell's equations reduce to:

$$\nabla \times \mathbf{E} = -\partial_t \cdot \mathbf{B} \qquad \nabla \mathbf{B} = 0$$

$$\nabla \times \mathbf{B} = \mu_0 \mathbf{J}$$

We have assumed that the field is quasi-static and that the plasma is approximately neutral.

Let us now look at the possible simplifications:

Geometry: The flow and the electromagnetic field are axisymetric. There is no externally imposed magnetic field. The Magnetic field is therefore azimuthal.

The Ohm's Law and the electromagnetic equations are combined in order to eliminate $\mathbf{E}$ and $\mathbf{J}$. One obtains an equation in $\mathbf{B}$ that describes the diffusion and convection of the magnetic field in a conducting medium:

$$\nabla \times (-\mathbf{u} \times \mathbf{B} + \frac{\nabla \times \mathbf{B}}{\mu_0 \sigma} + \frac{(\nabla \times \mathbf{B}) \times \mathbf{B}}{\mu_0 e n_e} - \frac{\nabla P_e}{e n_e}) = -\partial_t \mathbf{B}$$

Rewriting the equation in non-dimensional form,

$$-\partial_t^* \mathbf{B}^* + \nabla^* \times (\mathbf{u}^* \times \mathbf{B}^*) =$$

$$\frac{1}{R_m}\nabla^* \times (\frac{\nabla^* \times \mathbf{B}^*}{\sigma^*} + H_a(\frac{(\nabla^* \times \mathbf{B}^*) \times \mathbf{B}^*}{n_e^*} - \frac{\beta}{2}\frac{\nabla^*(n_e^* T_e^*)}{n_e^*}))$$

introduces three non-dimensional numbers: $N_1 = \frac{1}{R_m}$ for the magnetic diffusion due to conductivity; $N_2 = \frac{H_a}{R_m}$ for the non linear Hall effect; $N_3 = \frac{\beta H_a}{2R_m}$ for the electron diffusion. $R_m = \mu_0 \sigma_0 u_0 L_0$ is the magnetic Reynolds number, based on the distance between the electrodes; H_a is the Hall parameter;

$$H_a = \frac{B_0 \sigma_0}{e n_{e0}} = \omega_{ce} \tau$$

where ω_{ce} is the electron cyclotron angular frequency and $\tau_e = 1/\nu_e$ is the electron collision time . β is the plasma-β; ratio of the pressure to the magnetic pressure,

$$\beta = \frac{2\mu_0 P_e}{B_0^2}$$

The values of these non-dimensional numbers give an indication of the relative importance of each phenomenon: Inside the channel $N_1 \approx 0.5$, $N_2 \approx 0.6$, $N_3 \approx 0.03$. Therefore we take the Hall effect and the convection into account, but we neglect the effect of the electron pressure gradient on the conductivity. (Notice that a magnetic Reynolds Number based on the channel length would be of order 5 to 10).

Constant temperature approximation: In a plasma like the one considered here, the energy equation is the most difficult to justify. At high temperature (around 12500 K) the gas is strongly ionized and radiates energy. These processes are not necessarily in equilibrium and therefore cannot be accurately described by the energy conservation equation used in the fluid theory at low temperatures. As in most MHD models the energy conservation equation will be dropped and replaced with the assumption that the plasma is roughly isothermal. This assumption can be justified by the effect of ionization which tends to oppose any change in temperature by a displacement of the ionization equilibrium, by the thermal conductivity of the plasma, and by the value of the pressure relative to the magnetic pressure $\beta \ll 1$. The non-dimensional number describing the balance between kinetic energy and heat conduction (equivalent of the Reynolds number for the energy equation) is:

$$C_l = \frac{L_0 \rho_0 U_0^3}{\kappa T_0}$$

Its value goes from $\approx$ 200 in the cathode jet, to $\approx$ 1 along the external surface of the anode.

Conductivity: In the Spitzer-Härm aproximation the conductivity of a fully ionized plasma is proportional to $T^{\frac{3}{2}}$. Consequently we have a constant value for the electrical conductivity $\sigma = 3800$Si/m.

Even though the enrgy balance is not written, the fact that one part of the electrical work $\mathbf{E} \cdot \mathbf{J}$ is dissipated ohmically as $\frac{j^2}{\sigma}$ is implicit in the rest of the formulation, and therefore a meaningful thruster efficiency can be computed. What is ignored is the ultimate fate of the ohmic heat and its apportionment to ionisation, heat conduction, radiation, etc.

Since ionization processes are not covered in the model, the plasma is considered fully ionised when it enters the inlet of the accelerator.

Although the real Reynolds number is of the order of 100 to 200, the plasma is considered inviscid, which means that second order derivatives appear only in the electromagnetic equation.

The final set of equations after simplifications is then:

$$\partial_z(\rho u_z) + \frac{1}{r}\partial_r(r\rho u_r) = 0$$

$$\partial_z(\rho u_z u_z + P + \frac{B^2}{2\mu_0}) + \frac{1}{r}\partial_r(r\rho u_z u_r) = 0$$

$$\partial_z(\rho u_z u_r) + \frac{1}{r}\partial_r(r(\rho u_r u_r + P + \frac{B^2}{2\mu_0})) + \frac{-P + \frac{B^2}{2\mu_0}}{r} = 0$$

$$P = \rho R T_0$$

$$\oint \mathbf{E}d\mathbf{l} = 0$$

$$E_z = \frac{1}{\mu_0\sigma}\frac{1}{r}\partial_r rB - \frac{B}{\mu_0 e n_e}\partial_z B - u_r B$$

$$E_r = -\frac{1}{\mu_0\sigma}\partial_z B - \frac{B}{\mu_0 e n_e}\frac{1}{r}\partial_r rB + u_z B$$

The boundary conditions were taken as follows:

The tangential electric field is zero on the electrodes. The electrodes include the conducting surfaces of the anode and the cathode. The voltage drop across the plasma-sheath, which extends over a few Debye lengths inside the plasma, will be neglected. Consequentely the voltage drop across the channel will be underestimated when the anode is starved, i.e. at high current densities.

The entrance surface (the back plate) is an insulating surface which carries the injector holes. It is assumed that the gas is injected uniformly across the back plate, which would be the case with a porous back plate or with a plate containing a large number of injector holes. A transition between the gas state, characterized by a low temperature and a low conductivity, and the plasma state, where the gas is ionized and is a good conductor of electricity, arises once the gas is in the annular chamber. This ionization takes place in a region close to the back plate surface. The calculation starts after the ionization layer assuming that the gas has reached a uniform temperature of 12500 K, at which the electrical conduction is sufficently high to consider the gas as a plasma. Across the entrance plane the magnetic field is: $B = \mu_0 I/2\pi r$. The dynamic variables $\rho, \rho u_z, \rho u_r$ are specified along the entrance surface : $\rho u_r = 0$; ρu_z is specified by the mass flow rate:

$$\rho u_z = \frac{\dot{m}}{A_{intake}}$$

The existence of a steep density gradient immediately adjacent to the back plate makes it very difficult to resolve this layer numerically. Fortunately one of us has shown [22] that the details of the inlet gradients have only a small influence downstream. In our calculation we assign an arbitrary value to ρ.

On the outer boundary of the computational domain (i.e. far into the plume) $B = 0$. This condition means that there is no current going outside the boundary of the calculation, which is therefore an insulating surface. There are no gradients of ρ, ρu_z, ρu_r along the direction parallel to the flow.

On the axis of symetry $B = 0$.

Numerical Method

The system of equations is solved by the Newton-Raphston method using the technique of Finite Volumes for the discretization of the equations of motion, and a technique similar to the method of finite volumes for the magnetic field. Artificial viscosity is added to the equations of motion in order to avoid non-linear instabilities at places of strong density gradients. The conservation equations are discretized according to the method of finite volumes: The computational space is divided into 20×41 quadrilaterals. The grid is shown in figure 1. The variables $(\rho, \rho u_z, \rho u_r, B)$ are approximated by their space-average on each quadrilateral. The equations are written in their integral form:

$$\oint_S \rho \mathbf{u} d^2\mathbf{S} = 0$$

$$\oint_S (\rho\overline{\overline{uu}} - \overline{\overline{S}} - \overline{\overline{M}})d^2\mathbf{S} = 0$$

where the the tensor $\rho\overline{\overline{uu}} - \overline{\overline{S}} - \overline{\overline{M}}$ has the following physical components in cylindrical coordinates (z, r, ϕ) :

$$\begin{bmatrix} \rho u_z u_z + P + \frac{B^2}{2\mu_0} & \rho u_z u_r & 0 \\ \rho u_z u_r & \rho u_r u_r + P + \frac{B^2}{2\mu_0} & 0 \\ 0 & 0 & P - \frac{B^2}{2\mu_0} \end{bmatrix}$$

Since the problem is axisymetrical, the volume elements are obtained by rotating the quadrilaterals that define the grid cells by an infinitesimal angle $\Delta\phi$ around the axis of symetry. The surface integral around each element is broken into six integrals, one for each facet. Each of them is discretized by assuming that the fluxes are constant on each facet of the boundary. For the electro-magnetic field one uses a different integral (line integral over a closed contour):

$$\oint_C \mathbf{E}d\mathbf{l} = 0$$

The contours are defined by the same quadrilaterals as above. For each iteration the Newton-Raphson algorithm

inverts a matrix of order 3200 which represents the system of partial differential equations linearized at the current estimate of the solution vector. This takes about 10 minutes on a microVax. One needs about 10 iterations to attain convergence.

Experimental Background

Experimental studies have identified three modes of operation for the plasma accelerator: electrothermal mode, for which the dominant acceleration mechanism is the expansion of the heated gas across the thermodynamic pressure gradient; electromagnetic mode, for which the dominant acceleration mechanism is the expansion of the gas across the magnetic pressure gradient; finally the unstable regime which set on when the critical ratio $\frac{I^2}{\dot{m}}$ is exceeded. For argon as propellant, Hügel [11] gives an empirical value for the limiting current,

$$\frac{I^{*2}}{\dot{m}} \approx 2.5\ 10^{10} \qquad (\mathrm{A^2\ kg^{-1}\ s}),$$

which gives a current of the order of 12 kA for $\dot{m} = 6$ g/s. More recent work at Princeton and elsewhere has raised this by factors of up to 3, depending on the geometry and the injector configuration. An onset prediction based on the total starvation of the anode was proposed by Baksht, Moishes and Rybakov [3],

$$\frac{I^7 m_i^2}{\dot{m}^4} = \frac{945}{8} \frac{ekT}{\sigma \mu_0^4} \frac{LH^8}{d^5}$$

which leads to a critical value of 19 kA for our geometry.

An explanation which does not include the Hall effect has been proposed by Lawless and Subramanian [19], based on the mechanism of an excessive back EMF induced by a strong convective effect $\mathbf{u} \times \mathbf{B}$ in the opposite direction of the applied driving field $\mathbf{E}$. Neglecting the Hall effect they obtained, from a one-dimemsional analysis, an expression for the limiting current:

$$\frac{I^{*2}}{\dot{m}} \approx 8.52 \frac{a^*}{\mu_0} \qquad (\mathrm{A^2\ kg^{-1}\ s})$$

where a^* is the speed of sound at the choking point and μ_0 is the permeability of the vacuum. This gives a current of the order of 20 kA for $a^* = 10^4$ m/s and $\dot{m} = 6$ g/s. However the physical basis of their argument is open to criticism [22].

Assuming that the magnetic field is confined between two coaxial cylindrical electrodes and does not extend outside the exit plane of the thruster, one can integrate the effects of the Maxwell stress tensor, and one can predict the thrust due to the electro-magnetic effects by the formula:

$$T_{em} = \frac{\mu_0 I^2}{4\pi} \ln \frac{r_a}{r_c}$$

(11 Newton at 10kA for $\frac{r_a}{r_c} = 3$) The ratio $\frac{T_{em}}{\dot{m}}$ gives the exit velocity c_e.

The voltage is expected to be linear with the current for low currents (Joule heating), and to increase at a higher rate for high currents as the field accelerates the plasma and competes against the induced back EMF, showing a cubic dependence with the intensity.

Results

We have run fully coupled calculations for a mass flow rate of 6 grams per second and for various electrical currents between 0 and 10kA. Uncoupled calculations (i.e. calculating the electromagnetic field with a frozen flow field) have been obtained for currents between 0 and 100 kA.

A maximum of the magnetic field is observed along the cathode. Figure 2 shows the contours of constant rB. For an axisymetrical geometry these lines also represent the lines of current. The influence of the magnetic field on the conductivity tensor (Hall effect), is seen in the way the current lines concentrate at the tip of the anode and at the root of the cathode. As the current increases this effect becomes more pronounced. This effect can also be observed on figure 3, which shows the current density at the electrodes.

Figures 4 and 5 show the density contours for 0 and 10kA. For 10kA (figure 5) the density shows strong gradients and large fluctuations. At the inlet the density drops abruptly over a few cells. The compression of the plasma, under the influence of the Lorentz force (inward pinching effect), can be observed along the cathode and along the axis of symetry. Figure 6 shows an enlargement of the density plot for 10kA, where one observes: the compression of the plasma along the cathode; the strong rarefaction that follows the expansion of the plasma around the cathode corner, which reaches a minimum of 1.5 10^{20} m^{-3}; the recompression along the axis of symetry, where the density reaches a maximum of 108. 10^{20} m^{-3} at a distance of 1 cm from the tip of the cathode. On the anode side the plasma expands monotonically from 33. 10^{20} m^{-3} to 0.15 10^{20} m^{-3}. Figure 7 shows the density across the thruster along three different rows of cells. It shows the considerable increase in density in the cathode jet, downstream of the cathode along the axis of symetry.

A plot of the velocity vector obtained for 10kA (figure 8) shows a strong acceleration in the surface layer that surrounds the cathode. The existence of this layer can be inferred from the high values of both the electric field and the current density along the cathode (about an order of magnitude higher than at the anode).

The plot of the Hall number $\frac{B\sigma}{en_e}$ (figure 9) shows considerable gradients on the anode and cathode tips. These gradients are related to the electron density gradients created by the expansion of the plasma as it follows the electrode surfaces. The Hall effect (Tensorial conductivity) is likely to be responsible for the computational instabilities encountered at higher currents along the electrode surfaces.

The thrust was computed for various currents and is listed in table 2. The thrust increase due to the current is apparently very modest (9.8 N at 10kA), but is comparable to the thrust due to the Maxwell stress tensor predicted by the formula :

$$T_{em} = \frac{\mu_0 I^2}{4\pi} \ln \frac{r_a}{r_c}$$

(11 N at 10kA for $\frac{r_a}{r_c} = 3$). Thus the thruster is still operating at this condition mainly in the electrothermal regime.

Conclusions

The calculation of the MHD model was done for three values of the current: 0, 5kA and 10kA. The model does not converge above 10kA. The probable cause of the computational instability is the excessive value of the Hall parameter along the surfaces where rarefaction is present. Above a certain value of the current this rarefaction will be increased by the action of the Lorentz force, leading to a failure of the model along the boundaries.

The same cause may be responsible for the onset of instabilities observed in experimental devices. (The onset current expected from Hügel's formula is 12kA, the value from the Baksht et al. is 19kA, and the value from Lawless and Subramanian is 20kA).

The artificial damping introduced in the equation of motion in order to obtain a reasonably well-posed problem modifies the solution by an amount that reaches 5 percent of the momentum flux (for 10kA). The largest contribution to this error appears at the sharp turn around the anode corners.

References

[1] T. Ao, T. Fujiwara, "Numerical and Experimental Study of an MPD Thruster" *Proceeding of the 17th International Electric Propulsion Conference* Tokyo 1984, IEPC 84-08.

[2] G.V. Babkin, V.G. Mikhalev, S.N. Ogorodnikov, R.V. Orlov, A.V. Potapov, "High Current Coaxial Plasma Source", Sov. Phys. Tech. Phys. , Volume 20, 1975, pp 1175-1178.

[3] F.G. Baksht, B.Y. Moishes, A.B. Rybakov, "Critical Regime of a Plasma accelerator", Sov. Phys. Tech. Phys., Vol. 18, No. 12, June 1974, pp 1613-1616.

[4] R. D. Bühler "Plasma Propulsion for Near Earth Missions of Large Space Structures. Status, Problems and Prospects." Institut für Raumfahrtantriebe, Universität Stuttgart, IRA - 82 P 7

[5] I.S. Corry, R.G. Jahn, "Mass, Momentum and Energy Flow from an MPD Accelerator", Princeton University, Aerospace and Mechanical Sciences Report No. 999, 1971

[6] J.J. Dongara, C.B. Moler, J.R. Bunch, G.W. Stewart "LINPACK Users' Guide", SIAM.

[7] M. Drela, "Two-Dimensional Transonic Aerodynamic Design and Analysis Using the Euler Equations", GTL Report No. 187, Massachusetts Insitute of Technology, February 1986.

[8] M.B. Giles, "Newton Solution of Steady Two-Dimensional Transonic Flow" PhD Thesis, Department of Aeronautics and Astronautics, MIT, June 1985.

[9] J.M.Hoell, J. Burlock, O. Jarrett, "Velocity and Trust Measurements in Quasi-Steady Magneto-Plasma-Dynamic thruster", AIAA paper No. 70-1080.

[10] H. Hügel, Flow Rate Limitations in the Self-Field MPD Accelerator", AIAA paper No. 73-1094.

[11] H. Hügel, "Zur Funktionsweise der Anode im Eigenfeldbeschleuniger", Deutsche Forschungs- und Versuchsanstalt für Luft- und Raumfahrt, DFVLR-FB 80-20

[12] R.G. Jahn, "Pysics of Electric Propulsion", Chapters 8 and 9, McGraw-Hill, 1968.

[13] R.G. Jahn, A.J. Kelly, "Quasi-Steady Magnetoplasmadynamic (MPD) Thruster Performance Development", Princeton University, Department of Mechanical Engineering and Applied Science, MAE Report No. 1507d, March 1983.

[14] A. Jameson, W. Schmidt, E. Turkel, "Numerical Solution of the Euler Equations by Finite Volume Methods Using Runge-Kutta Time-Stepping Schemes." AIAA-81-1259

[15] A. Jameson, S. Yoon, "Multigrid Solution of the Euler Equations Using Implicit Schemes", AIAA paper No. 85-0293.

[16] D. C. Jespersen, "Recent Developments in Multigrid Methods for the Steady Euler Equations", Von Karman Inst. for Fluid Dynamics, CFD Volume 2 1984.

[17] I. Kimura, K. Toki, M. Tanaka, "Current Distribution on the Electrodes of MPD Arcjets", AIAA Journal. Vol. 20, No. 7, July 1982.

[18] K. Kuriki, H.Suzuki, "Thrust Measurment of Quasi-Steady MPD Arcjet", AIAA paper No. 76-1002.

[19] J.L. Lawless, V.V. Subramanian, "A Theory of Onset in MPD-Thrusters, AIAA paper 85-2039.

[20] H. Lien, R.L. Garrison, " System Trade-offs for Pulsed MPD Thruster in Space Mission Application ", AIAA paper No. 72-457.

[21] A.C. Malliaris, R.R. John, R.L. Garrison, D.R. Libby "Quasi-Steady MPD Propulsion at High Power", NASA CR-111872.

[22] M. Martines-Sanches, "Structure of Self Field Accelerated Plasma Flows", AIAA paper 87-1065.

[23] R. Peyret, T. D. Taylor," Computational Methods for Fluid Flow", Springer Verlag, pp 108-112.

[24] T.H.Pulliam, J.L. Steger, "Recent Improvements in Efficiency, Accuracy and Convergence for Implicit Approximate Factoriization Algorithms", AIAA Paper No 85-0360.

[25] R.P. Reklis, R.J. Conti, "Computational Probing of Hypersonic Laminar Wake", AIAA Paper No. 84-1579.

[26] P.J. Roache, "On Artificial Viscosity", Journal of Computational Physics, Vol.10, No.2, October 1972.

[27] M. Tanaka, I. Kimura, Y. Arakawa, "Current Distribution on the Electrodes of MPD Arcjets with Applied Magnetic Field", AIAA Paper, No. AIAA-82-1918, 1982

[28] M. Tanaka, I. Kimura, "Theoretical Analysis of Current Distribution and Plasma Acceleration in MPD Arcjet" *Proceeding of the 17th International Electric Propulsion Conference* Tokyo 1984, IEPC 84-07.

[29] P.J. Turchi, R.G. Jahn, "The Cathode Region of a Quasi Steady MDP Arcjet", AIAA Paper No. 70-1094.

Symbols

a^*	Speed of sound at chocking point in the theory of Lawless and Subramanian
B	Magnetic field (T)
c_e	Exit velocity
C_l	Non dimensional parameter in the energy equation (Clausius Number)
d	distance between electrodes
e	Charge of the proton
E	Electric field ($V\ m^{-1}$)
E_{EM}	Electromagnetic energy per unit volume
E_I	Internal energy per unit volume
E_K	Kinetic energy per unit volume
H	Average perimeter of the inlet
H_a	Hall parameter
I^*	Current at the threshold of the turbulent regime.
J	Current density ($A\ m^{-2}$)
k	Boltzman constant
L	Average length of the channel
m_i	Molecular mass of the gas (kg)
$\overline{\overline{M}}$	Maxwell stress tensor ($N\ m^{-2}$)
$\dot{m}$	Mass flow rate of the propellant ($kg\ s^{-1}$)
m_z, m_r	Z- and r-momentum ($= \rho u_z, \rho u_r$)
n_e	Density of electrons (m^{-3})
P	Pressure ($N\ m^{-2}$)
q	Heat flux ($W\ m^{-2}$)
R	Gas constant ($J\ kg^{-1}\ K^{-1}$)
R_m	Magnetic Reynolds number
$\overline{\overline{S}}$	Stress tensor ($N\ m^{-2}$)
T	Temperature (K)
u	Velocity ($m\ s^{-1}$)
$\overline{\overline{uu}}$	Diad ($u_i u_j$ in cartesian coordinates)
β	Plasma-Beta (pressure/magnetic pressure)
γ	Specific heat ratio
κ	Heat conductivity
μ_0	Permittivity of vacuum
ρ	Mass density ($kg\ m^{-3}$)
σ	Conductivity ($Si\ m^{-1}$)
τ_e	Electron collision time
ϕ	Axisymertic coordinate
ω_{ce}	Electron gyrofrequency (angular)

Cathode radius	r_c	2. cm
Anode radius	r_a	6. cm
Cathode length		6. cm
Anode length		12. cm
Inlet density	ρ_{inlet}	2.21 10^{-4} kg m^{-3}
Inlet pressure	P_{inlet}	1144 Pa
Inlet velocity	Uz_{inlet}	2700 m/s
Inlet X-sec. area	A_{inlet}	10^{-2} m^2
Temperature	T_0	1.25 10^4 K
Conductivity	σ_0	3.8 10^3 Si/m
Mass flow rate	$\dot{m}$	6 g/s
Current	I	(0., 5., 10.) kA
Gas constant	R	0.416 kJ/kg/K

Table 1: Parameters for the Calculations

RESULTS OF THE MODELS

Current (kA)	Voltage MHD model (V)	Thrust (MHD) (N)	Isp (MHD) (km/s)
0.		30.2	5.0
5.	6.7	32.2	5.4
10.	16.2	40.	6.7

Table 2: Results

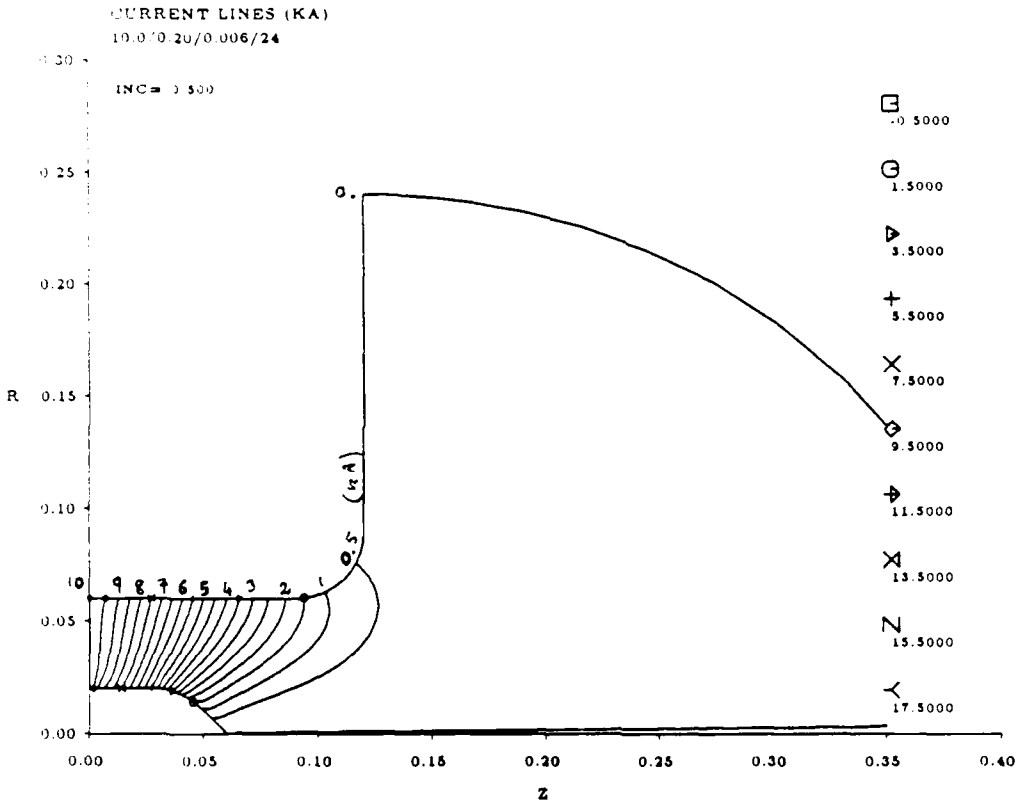

Figure 2: Current lines for $I = 10kA$ (Calculation)

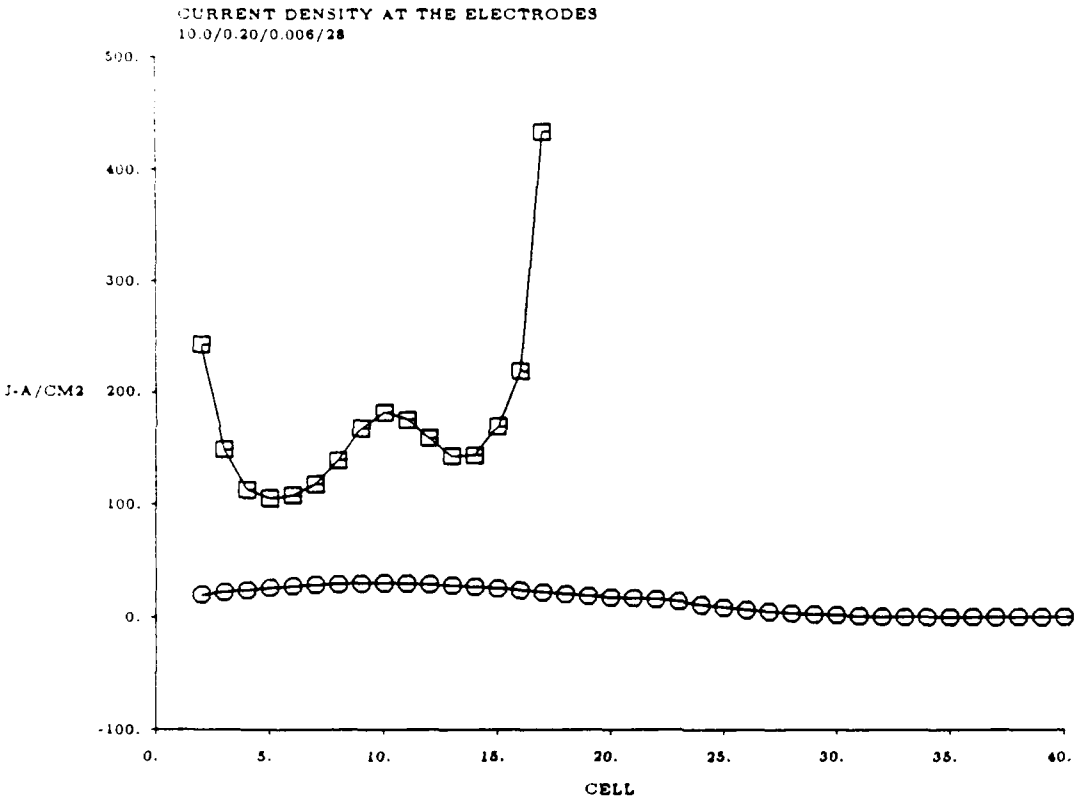

Figure 3: Current density at the electrodes for $I = 10kA$ (Calculation)

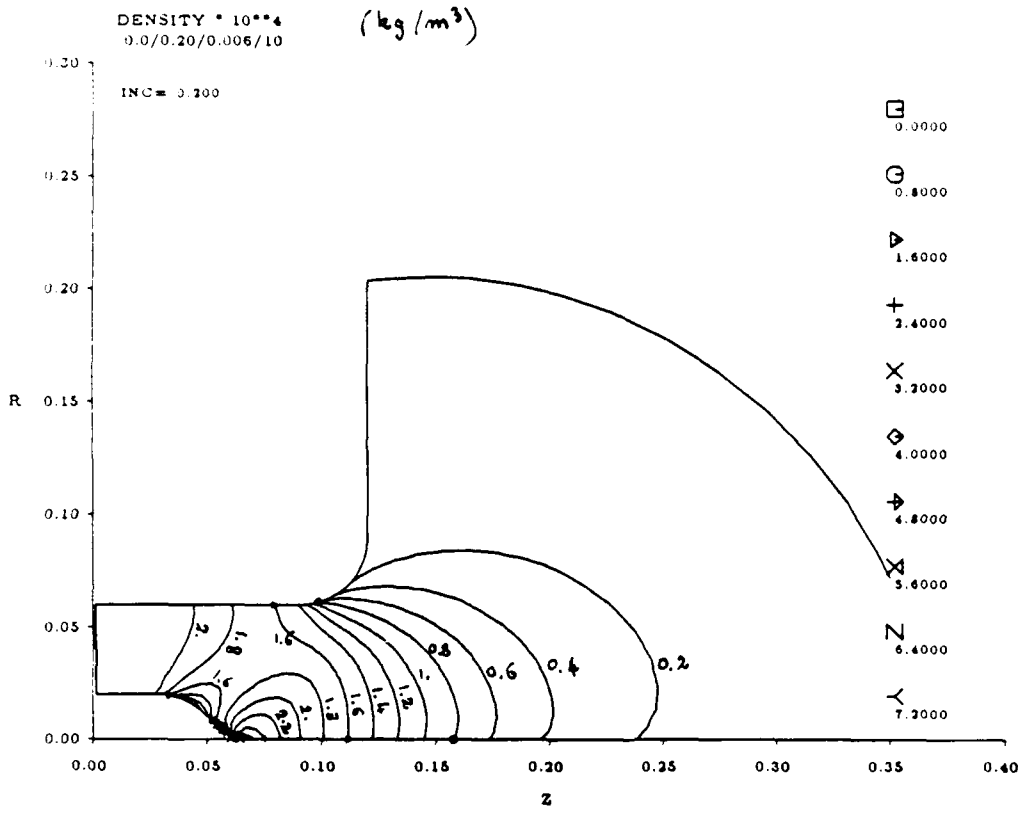

Figure 4: Density for $I = 0kA$ (Calculation)

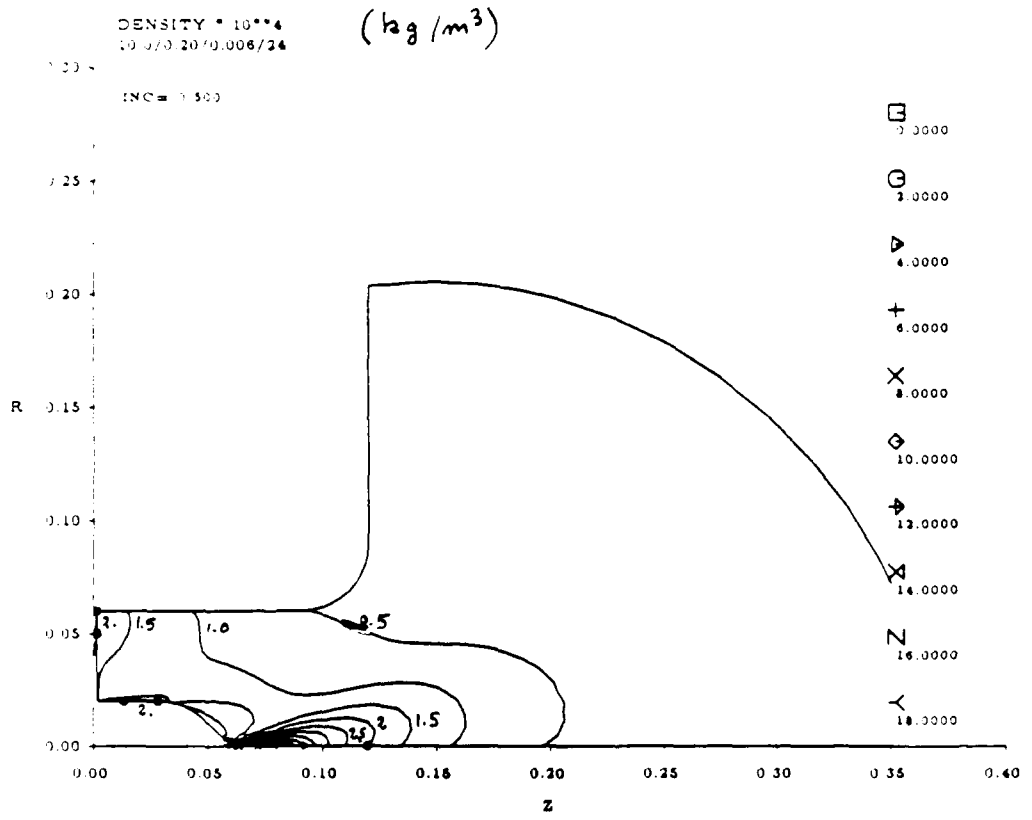

Figure 5: Density for $I = 10kA$ (Calculation)

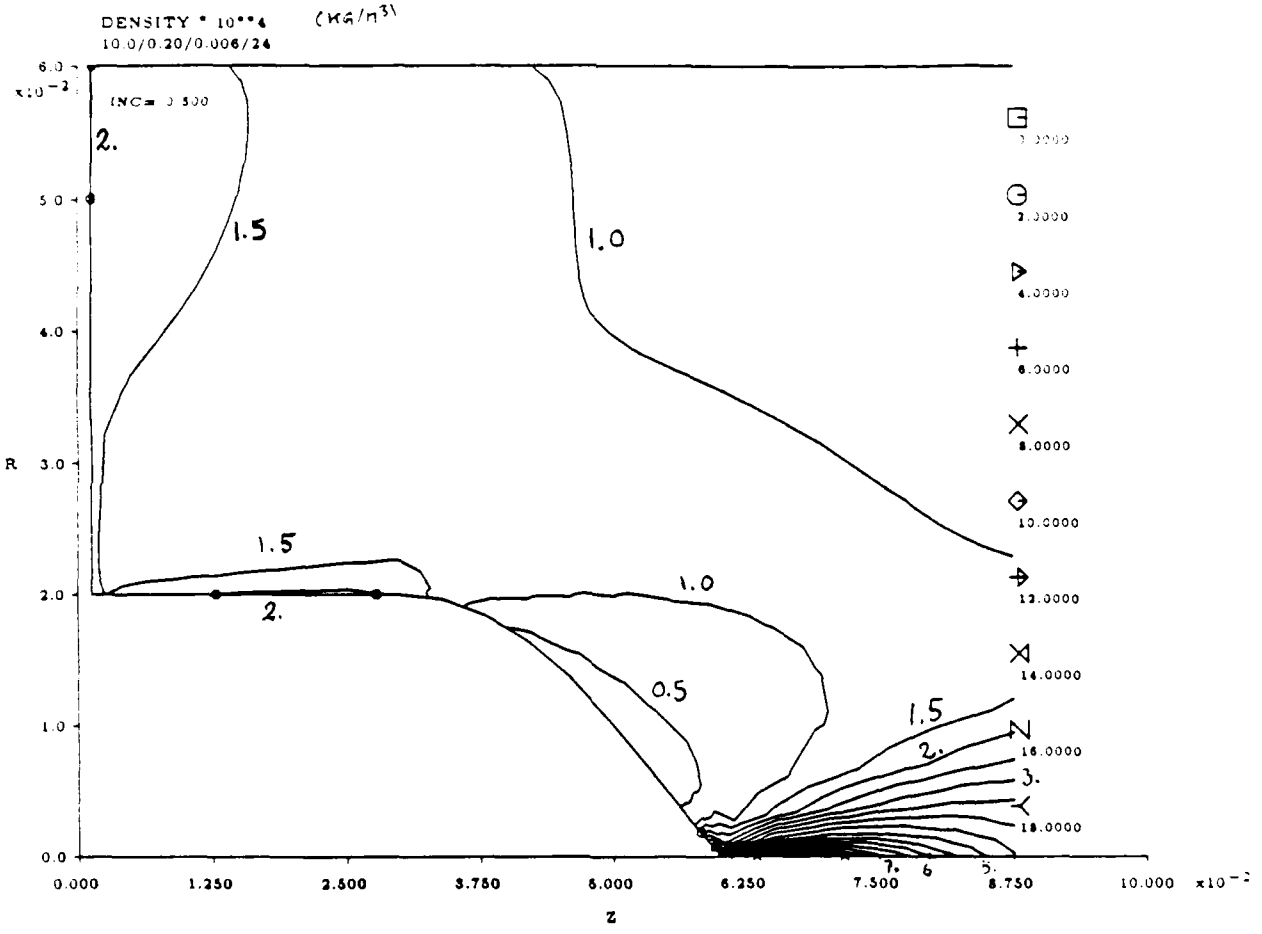

Figure 6: Density for $I = 10kA$ (Calculation)

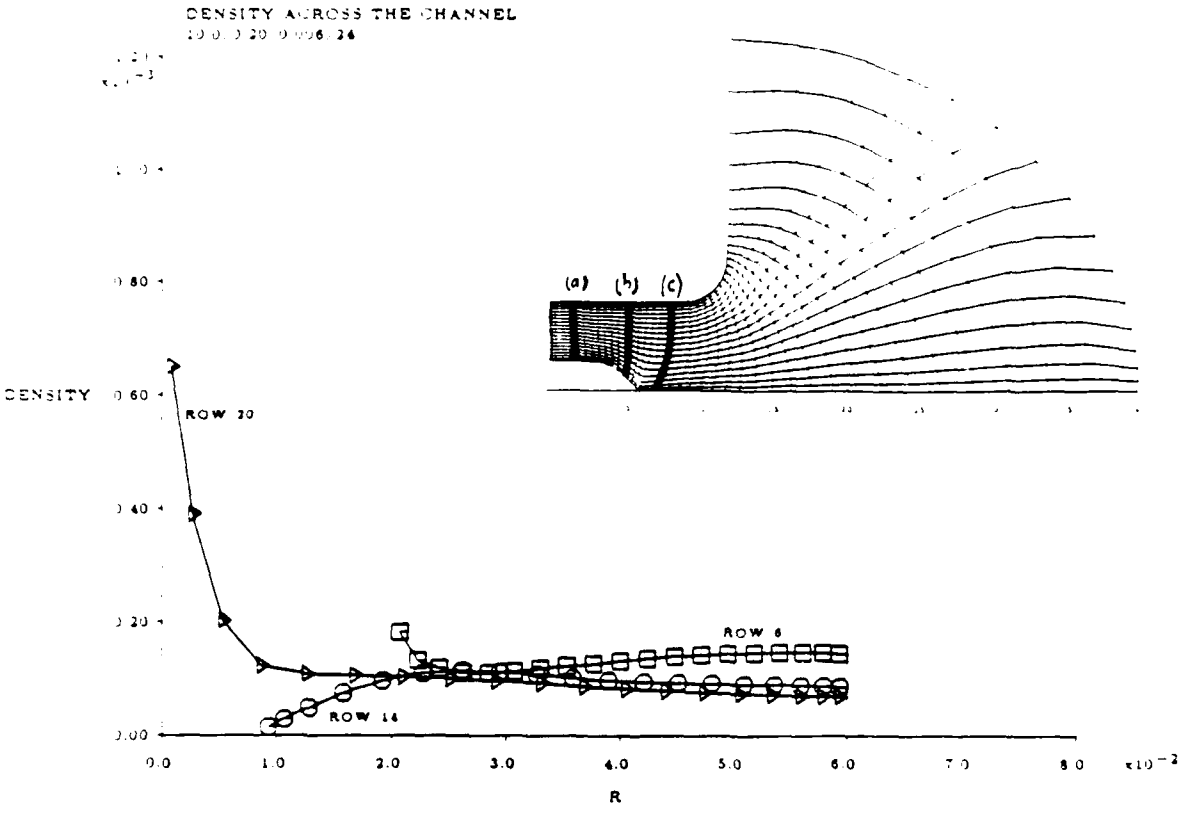

Figure 7: Density across the channel for $I = 10kA$ (Calculation) (a) 6th row of cells (inside the channel); (b) 14th row of cells (end of the cathode); (c) 20th row of cells (beyond the tip of the cathode).

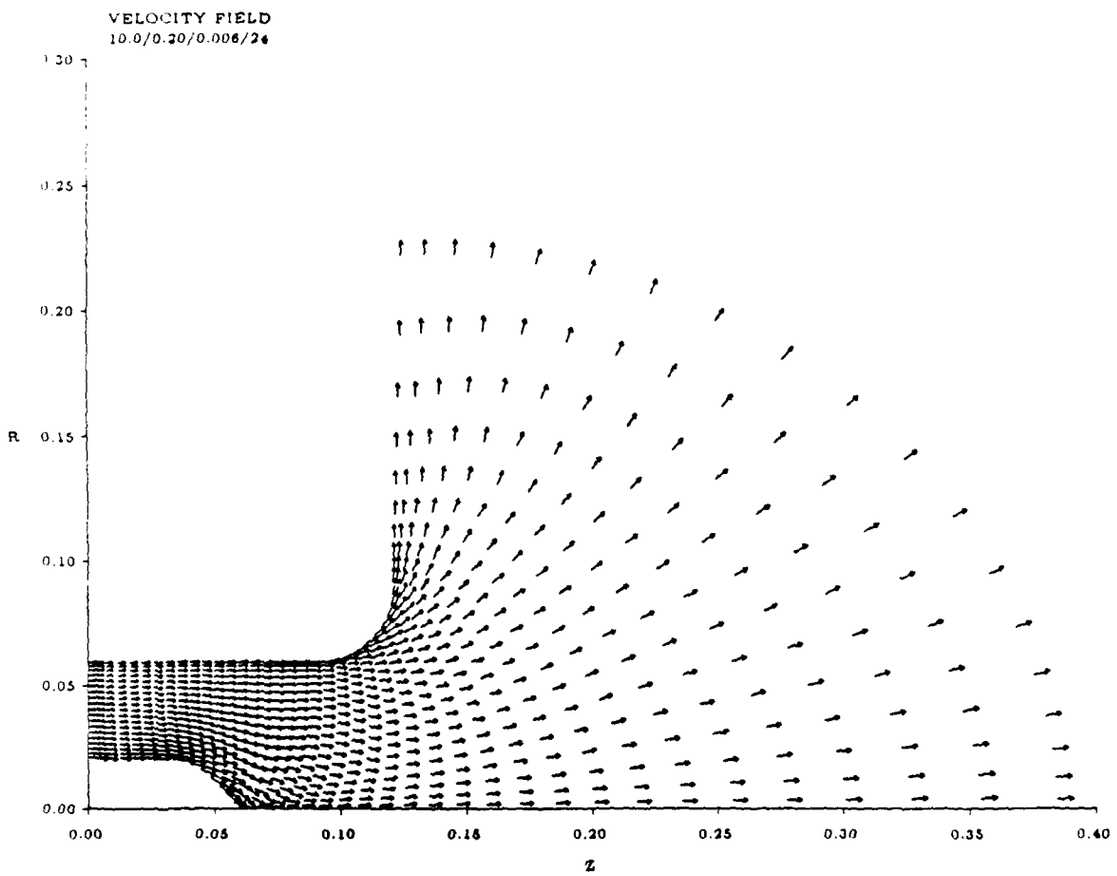

Figure 8: Velocity vectors for $I = 10kA$ (Calculation)

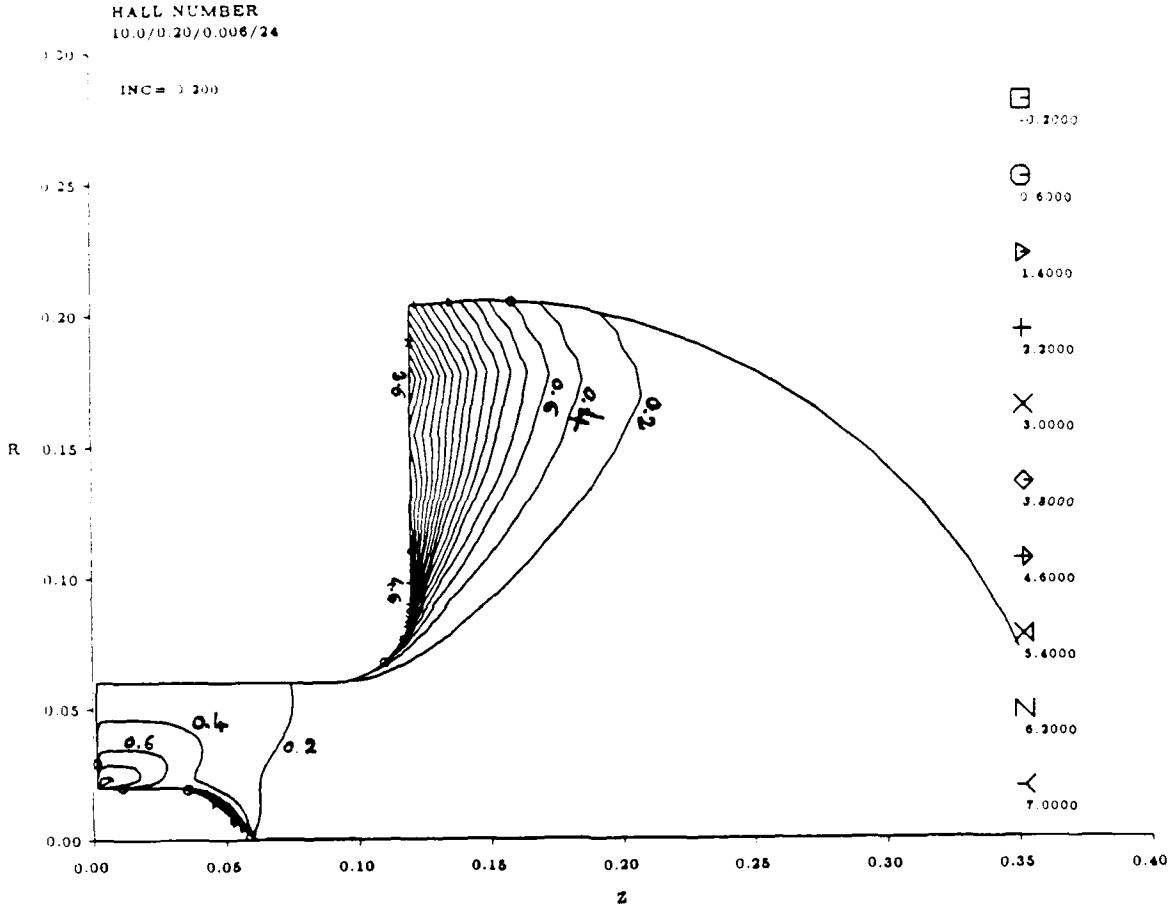

Figure 9: Hall number H_a for $I = 10kA$ (Calculation)